HIF1{alpha} modulates reprogramming through early glycolytic shift and up-regulation of PDK1-3 and PKM2

Prigione, A., Rohwer, N., Hoffman, S., Mlody, B., Drews, K., Bukowiecki, R., Bluemlein, K., Wanker, E.E., Ralser, M., Cramer, T., Adjaye, J.

Title: HIF1α modulates reprogramming through early glycolytic shift and up-regulation of PDK1-3 and PKM2

Authors and affiliations: Alessandro Prigione[1,2§], Nadine Rohwer[3], Sheila Hoffman[2], Barbara Mlody[1], Katharina Drews[1], Raul Bukowiecki[1,2], Katharina Blümlein[4], Erich E. Wanker[2], Markus Ralser[4], Thorsten Cramer[3], James Adjaye,[1,5§]

[1]Molecular Embryology and Ageing Group, Department of Vertebrate Genomics, Max Planck Institute for Molecular Genetics, Berlin, Germany

[2]Department of Neuroproteomics, Max Delbrueck Center for Molecular Medicine (MDC), Berlin, Germany

[3]Medizinische Klinik mit Schwerpunkt Hepatologie und Gastroenterologie, Campus Virchow-Klinikum, Charité-Universitätsmedizin Berlin, Berlin, Germany

[4]Department of Biochemistry and Cambridge Systems Biology Centre, University of Cambridge, UK

[5]Institute for Stem Cell Research and Regenerative Medicine, Medical Faculty, Heinrich Heine University, Duesseldorf, Germany

[§]**Contact information**: Alessandro Prigione, M.D. Ph.D. Robert-Roessle-Str. 10 D-13125 Berlin-Buch, Germany, Tel: 0049-30-9406-2871, Fax: 0049-30-9406-3696, Email: alessandro.prigione@mdc-berlin.de.

James Adjaye, Ph.D. Institute for stem cell research and regenerative medicine, Medical faculty, Heinrich Heine University, Duesseldorf, Germany,

Tel: 0049-211 81 08191, Fax: 0049-211 81 19147,

Email: James.Adjaye@med.uni-duesseldorf.de.

Running head: HIF1α associated metabolic switch in iPSCs

Author contribution:

Alessandro Prigione: Conception and design, Collection and assembly of data, Data analysis and interpretation, Financial support, Manuscript writing

Nadine Rohwer: Collection and assembly of data

Sheila Hoffman: Collection of data

Barbara Mlody: Collection of data

Katharina Drews: Collection and assembly of data

Raul Bukowiecki: Collection of data

Katharina Blümlein: Collection of data

Erich E. Wanker: Financial support

Markus Ralser: Data analysis and interpretation, Financial support

Thorsten Cramer: Data analysis and interpretation, Financial support

James Adjaye: Conception and interpretation, Financial support, Editing and final approval of the manuscript

Brief acknowledgements: The authors declare no competing financial or commercial interests and acknowledge support from the Max Planck Society. A.P. acknowledges support from the Fritz Thyssen Foundation (grant AZ. 10.11.2.160). M.R. is a Wellcome Trust Research Career Development and Wellcome-Beit fellow. J.A. acknowledges support from the German Federal Ministry of Education and Research (BMBF) grants (01GN1005), (01GN0807) and (0315717A), which is a partner of the ERASysBio+ initiative supported under the EU ERA-NET Plus scheme in FP7.

Keywords: reprogramming; iPS cells, metabolism; HIF1α; PDK1; PKM2

Abstract

Reprogramming somatic cells to a pluripotent state drastically reconfigures the cellular anabolic requirements, thus potentially inducing cancer-like metabolic transformation. Accordingly, we and others previously showed that somatic mitochondria and bioenergetics are extensively remodeled upon derivation of induced pluripotent stem cells (iPSCs), as the cells transit from oxidative to glycolytic metabolism. In the attempt to identify possible regulatory mechanisms underlying this metabolic restructuring, we investigated the contributing role of hypoxia-inducible factor 1 alpha (HIF1α), a master regulator of energy metabolism, in the induction and maintenance of pluripotency. We discovered that the ablation of HIF1α function in dermal fibroblasts dramatically hampers reprogramming efficiency, while small molecule-based activation of HIF1α significantly improves cell fate conversion. Transcriptional and bioenergetic analysis during reprogramming initiation indicated that the transduction of the four factors is sufficient to up-regulate the HIF1α target pyruvate dehydrogenase kinase (PDK) 1 and set in motion the glycolytic shift. However, additional HIF1α activation appears critical in the early up-regulation of other HIF1α-associated metabolic regulators, including PDK3 and pyruvate kinase (PK) isoform M2 (PKM2), resulting in increased glycolysis and enhanced reprogramming. Accordingly, elevated levels of PDK1, PDK3, and PKM2 and reduced PK activity could be observed in iPSCs and human embryonic stem cells (hESCs) in the undifferentiated state. Overall, the findings suggest that the early induction of HIF1α targets may be instrumental in iPSC derivation via the activation of a glycolytic program. These findings implicate the HIF1α pathway as an enabling regulator of cellular reprogramming.

Introduction

Oxygen concentration plays a critical role in mediating modifications of the cellular metabolic profile [1]. Under physiological normoxic conditions, human somatic cells are characterized by active mitochondria and oxidative phosphorylation (OXPHOS)-based metabolism, while oxygen-deprived cells exhibit increased conversion of glucose to lactate (the "Pasteur effect"). However, tumor cells fine-tune their cellular bioenergetics to respond to higher cellular demands and can shift to glycolysis-based metabolism even in the presence of high level of oxygen, a phenomenon known as aerobic glycolysis or "Warburg effect" [2, 3]. This metabolic shift seems apparently counter-intuitive given the low efficiency of glycolytic metabolism in terms of generation of ATP molecules. Nevertheless, several lines of evidence demonstrate that this metabolic adaptation endows proliferative cells with critical advantages.

First, anabolic pathways branching out from the glycolytic path supply the intermediates for cell growth, including amino acids and lipid precursors [4, 5]. Thus, rapidly dividing cells, such as cancer cells, increase the flux through glycolysis to satisfy their need of macromolecules, by enhancing glucose uptake and by slowing the entry of pyruvate into mitochondria [6]. Second, the energy reconfiguration can provide protection against oxidative stress [5], by avoiding high levels of reactive oxygen species (ROS), common by-products of mitochondrial respiration, and by re-routing glycolytic intermediates into the pentose phosphate pathway, which generates not only essential nucleotide precursors but also the reducing factor NADPH, required for the activity of antioxidant enzymes [7]. Recent data on pyruvate kinase, which catalyzes the conversion of phosphoenolpyruvate (PEP) into pyruvate in the last step of the glycolytic cascade, support the idea that the Warburg effect may promote cellular redox homeostasis. Pyruvate kinase isoform M2 (PKM2) is highly expressed in cancer cells [8, 9] and upon oxidation it looses activity, thereby reducing pyruvate

formation and diverting the glycolytic flux into the pentose phosphate pathway, which eventually supports antioxidant activities [10-12].

A key mediator of the metabolic re-configuration occurring under low oxygen conditions is the transcription factor hypoxia-inducible factor 1 (HIF1) [13, 14]. HIF1 is a heterodimer consisting of a constitutively expressed HIF1 β subunit and an oxygen-regulated HIF1α, which is physiologically degraded under normoxic conditions by oxygen-dependent prolyl-hydroxylases (PHD1-3). When oxygen level decreases, or when PHD enzymes are pharmacologically inhibited, HIF1α protein escapes degradation and translocates in the nucleus, where it initiates a gene expression reprogramming ultimately leading to a switch from OXPHOS to glycolysis. HIF1α target genes include glucose transporters, to increase glucose uptake, and pyruvate dehydrogenase kinases (PDK1-3) [15-17], to shunt pyruvate away from the mitochondria through the inhibition of pyruvate dehydrogenase (PDH). In addition, HIF1α interacts with PKM2 and promotes its gene transcription [18], further implying an instructive role for HIF1α downstream signaling in the Warburg-like restructuring of glucose metabolism.

The derivation of induced pluripotent stem cells (iPSCs), allowing somatic cells to acquire embryonic stem cells (ESCs)-like features [19], is also associated with a profound re-configuration of anabolic demands. Indeed, induced pluripotent stem cells (iPSCs) show high proliferation rate and distinct cell cycle features compared to parental somatic cells [20]. This suggests that a corresponding reprogramming of energy metabolism may also be in place. Accordingly, we previously discovered that somatic mitochondria and cellular bioenergetics are extensively remodeled upon cellular reprogramming as the cells adopt a glycolytic metabolism [21]. Following these initial observations, several groups further confirmed that a Warburg-like metabolic reconfiguration takes place in both mouse and human iPSCs [22-26]. Indeed, the process of "metabolic reprogramming" is now being recognized as an emerging important step of the induction of pluripotency [27-30].

The metabolic switch of cell fate reprogramming does not appear to be due to dysfunctional mitochondria, which are in fact capable of respiring and consume oxygen, as demonstrated by bioenergetic profiling studies [25, 26, 31]. However, like cancer cells, proliferating pluripotent stem cells (PSCs) may opt for glycolysis as they necessitate building biomass and at the same time maintaining redox homeostasis. In accordance, PSCs exhibit up-regulation of genes involved in glucose uptake and the initial steps of glycolysis, increased expression of PDK1 [25, 31], suggesting the re-routing of metabolism outside of the mitochondria, and elevated levels of glucose-6-phosphate (G6P) [31], indicative of enhanced flux through the pentose phosphate pathway. Moreover, ROS levels are also reduced in PSCs and so is the amount of oxidative damage [21, 32]. Finally, exposure to hypoxic environment favorably supports self-renewal and pluripotency [33-35], enhances iPSC generation [36], and maintain hESCs in a more developmentally immature state [37].

Here, we sought to investigate the mechanisms underlying the metabolic reprogramming occurring upon cell fate transition and specifically dissect the contribution of the HIF1α pathway. We found that a small molecule mimicking HIF1α activation enhances reprogramming, while the ablation of HIF1α results in a dramatic loss of colony formation. By performing transcriptional and bioenergetic profiling during early reprogramming, we discovered that the transduction of the four factors is sufficient to up-regulate PDK1 and thereby initiating a glycolytic shift. The exposure to hypoxia or to HIF1α activation further stimulates the expression PDK3 and PKM2, resulting in increased early switch to glycolysis and more efficient iPSC generation. The additional up-regulation of PDK3 and PKM2 might be critical in enhancing reprogramming, since we observed that their expression is elevated in undifferentiated PSCs and is coupled to reduced PK activity, all traits associated with a glycolytic state. Taken together, early induction of HIF1α-associated glycolytic modulators may be instrumental in the establishment of pluripotency and may possibly represent an enabling regulatory step during cell fate conversion.

Materials and Methods

Cell lines and culture conditions

Neonatal foreskin fibroblasts (FFs) HFF1 and BJ were purchased from ATCC (# SCRC-1041 and #CRL-2522, respectively) and dermal fibroblasts (DFs) NFH2 were previously derived from an 84 year-old woman [38]. All fibroblasts were cultured using DMEM supplemented with 10% bovine serum, nonessential amino acids, L-glutamine, penicillin/streptomycin, and sodium pyruvate (all from Invitrogen, CA). All iPSC lines were previously generated using the four Yamanaka factors retroviral cocktail: HFF1-derived iPSCs (lines iPS2 and iPS4) [21], BJ-derived iPSCs (lines iB4 and iB5) [31], NFH2-derived iPSCs (lines OiPS3, OiPS6, OiPS8, and OiPS16) [38]. hESC lines H1 and H9 (WiCell) and iPSCs were cultured in hESCs media containing KO-DMEM supplemented with 20% knockout serum replacement, nonessential amino acids, L-glutamine, penicillin/streptomycin, sodium pyruvate, 0.1mM β-mercaptoethanol (all from Invitrogen, Carlsbad, CA), and 8 ng/ml bFGF (Prepotech, Rocky Hill, NJ). Pluripotent stem cells were harvested in feeder-free conditions using DMEM-F12 media supplemented N2/B27. All cultures were normally kept in a humidified atmosphere of 5% CO2 at 37°C under atmospheric oxygen condition (20%).

HIF1α activation

To generate hypoxic conditions, the oxygen concentration was set to 1% and the cells were maintained under hypoxia for 24h. A small molecule activator of HIF1α was employed, ethyl 3,4-dihydroxybenzoate (EDHB) (Sigma, #E24859), at a concentration of 100μM of, as previously shown [39]. To test the effect of HIF1α activation on the early reprogramming-initiating events, FFs were transduced twice with the four factor retroviral cocktail (OSKM), as previously described [40], alone or in combination with 100μM EDHB treatment. The cells were then harvested after 24h from the first transduction (4F 24h and 4F EDHB 24h), after

48h from the first transduction (that means 24h after the second transduction) (4F 48h and 4F EDHB 48h), and after 72h from the first transduction (4F 72h and 4F EDHB 72h). In addition, FFs were treated only with 100μM EDHB for 24h (EDHB 24h), 48h (EDHB 48h), and 72h (EDHB 72h).

HIF1α knockdown

To stably knockdown HIF1α, BJ fibroblasts were transduced with lentiviruses containing shRNA sequences against human HIF1α (BJ-HIF1-KD) and scrambled control oligonucleotides (BJ-SCR-KD) (TIB MOLBIOL, Berlin, Germany) [41]. Oligonucleotides were inserted into the lentiviral bicistronic vector pPR1, which allows for co-expression of GFP [42]. Recombinant lentiviruses were produced in 293T cells using the calcium-phosphate method. Human BJ fibroblasts stably expressing shRNAs were generated by double transduction with lentiviruses at a multiplicity of infection (MOI) of 10 for 24h. Transduction efficiency of target cells was determined by flow cytometry analysis of GFP using a FACSCalibur™ (Becton Dickinson, Heidelberg, Germany).

Cellular reprogramming

To test the consequences of HIF1α manipulation on the overall efficiency of iPSC generation, BJ fibroblasts, SCR-KD BJ fibroblasts, HIF1-KD BJ fibroblasts, and BJ fibroblasts treated with EDHB were reprogrammed to pluripotency using retroviral vectors expressing the four Yamanaka factors (4F: OCT4, SOX2, KLF4, and c-MYC), following our previously published protocol [21]. To test the effect of HIF1α knockdown on viral-free iPSC derivation, BJ fibroblasts, SCR-KD BJ fibroblasts, and HIF1-KD BJ fibroblasts were transfected using three non-integrative episomal plasmids containing a total of seven factors (4F plus NANOG, LIN28, and SVLT), as previously described [43]. Briefly, 8×10^5 fibroblasts (BJ, SCR-KD, and HIF1-KD) were nucleofected using the Amaxa Cell Line Nucleofector Kit (Lonza, Basel,

Switzerland). After nucleofection, fibroblasts were immediately mixed with 500µl DMEM medium before seeding into six-well plates. The following day, the cells were cultured using ESC medium supplemented with a small molecule cocktail composed by CHIR99021, A-83-01, PD0325901, and Y-27632 (all from Stemgent) [43]. Four weeks after either retroviral or plasmid reprogramming, the cells were fixed and stained for NANOG expression using the ABC method (see below). The reprogramming efficiency was defined as the number of NANOG positive colonies relative the total starting number of fibroblasts.

Global gene expression analysis

Biotin-labeled cRNA samples were produced as previously decribed [21] and hybridized onto Illumina human-8 BeadChips version 3 (Illumina, San Diego, CA, United States). The following samples were used: BJ, BJ-HIF1-KD, BJ-SCR-KD, 4F 24h, 4F 48h, 4F 72h (hybridized in duplicate), EDHB 24h, EDHB 48h, EDHB 72h, 4F EDHB 24h, 4F EDHB 48h, 4F EDHB 72h (hybridized in single). In addition, previously generated array data were incorporated in the analysis, including: amniotic fluid cells (AFCs), foreskin fibroblasts (FFs) (HFF1 and BJ), dermal fibroblast (DFs) (NFH2), hESC lines (H1 and H9), FFiPSC lines (iPS2, iPS4, iB4, and iB5), DFiPSC lines (OiPS3, OiPS6, OiPS8, and OiPS16) (all hybridized in duplicate) and AFiPSC (lines 4, 5, 6, 10, hybridized in single, and line 41, hybridized in duplicate) [21, 31, 38, 44]. Microarray analysis, PCA plot, and the general heatmap were performed using the *R*/Bioconductor package. Genes were considered significantly expressed with detection p values ≤ 0.01. Differential expression analysis was performed using the Illumina custom method, using differential p values ≤ 0.01, fold change ratio > 1.5. The heatmap for energy metabolism was generated using Microarray Software Suite TM4 (TMEV.bat) with an input list adapted from SA Biosciences PCR arrays (Human Glucose Metabolism PCR Array, www.sabiosciences.com). Pathway analysis was determined by mapping onto KEGG pathways using Database for Annotation, Visualization and Integrated

Discovery (DAVID) (http://david.abcc.ncifcrf.gov). Microarray results have been deposited in the GEO database (accession number GSE37709).

Quantitative real-time PCR (qPCR)

Real-Time PCR was performed in 384 or 96 Well Optical Reaction Plates (Applied Biosystems, Foster City, CA, United States) using SYBR®Green PCR Master Mix (Applied Biosystems). Reactions were carried out on the ABI PRISM 7900HT Sequence Detection System (Applied Biosystems). Duplicate or triplicate amplifications were carried out for each target gene with at least three wells serving as negative controls. Quantification was performed using the comparative Ct method (ABI instruction manual), normalized over *ACTB*, and presented as a log2 values with respect to the biological controls. The list of all primers used in this study is presented in Supp. Table 4.

Immunostaining and western blotting

Avidin-Biotin Complex (ABC) method was used to stain NANOG-positive hESC-like colonies, as described elsewhere [45]. Briefly, after primary incubation with NANOG antibody (1:100, Abcam #ab62734), biotinylated universal secondary antibody was applied following the manufacturer's instruction (Vector Laboratories, ABC universal kit #PK-6200). The ABC reagent was then added to bind HRP to the primary/secondary complex. HRP enzyme activity was then visualized using the chromogen substrate diaminobenzidine tetrachloride (DAB, Sigma # D5637). Senescence-associated β-galactosidase staining was performed according to the manufacturer's protocol (Cell Signaling, Danvers, MA, USA, www.cellsignal.com). Cells stained for NANOG or β-galactosidase were photographed using a digital camera (Canon).

For western blot analysis, nuclear protein extracts were prepared as described in details before [46], then resolved by electrophoresis on an 8% sodium dodecyl sulfate-polyacrylamide gel,

and transferred to a nitrocellulose membrane (Amersham Biosciences, Freiburg, Germany). Blots were probed with antibodies against HIF1α (AB1536; R&D Systems, Minneapolis, MN, USA), HIF2α (ab199, Abcam, Cambridge, UK), and YY1 (sc-281; Santa Cruz Biotechnology, Santa Cruz, CA, USA). Secondary antibodies were conjugated to Horseradish Peroxidase (Dianova, Hamburg, Germany) and peroxidase activity was visualized using the Western Lightning Chemiluminescence Reagent Plus (Perkin Elmer Life Sciences, Boston, Massachusetts, USA).

Absolute quantification (AQUA) of PKM1 and PKM2

The mass spectrometry-based AQUA approach was used to determine the absolute quantification of PKM1 and PKM2 isoforms, as previously described [8]. Briefly, protein samples from yeasts carrying p414TEF-PKM1 or p413TEF-PKM2, somatic cells, and pluripotent stem cells were separated on a 10% SDS-PAGE gels and the mass region between 50-70 kDa were excised. The gel pieces were then subjected to an "in-gel" tryptic digest. The AQUA peptide mixture (20 µL), containing all three AQUA peptides, was spiked to the samples as soon as the tryptic digest was completed. For quantitation of the tryptic peptides of interest, their corresponding AQUA analogue were spiked in the samples after the tryptic digest. Analysis was performed on a nanoLC (Eksigent, Ultra 2D) coupled online to a hybrid triple quadrupole/ion trap mass spectrometer (AB/SCIEX, QTRAP 5500). The identity of the quantified peptides was confirmed by collecting of MS/MS spectra on the QTRAP operating in iontrap mode. In order to confirm specificity of the selected tryptic peptides, yeasts expressing either only PKM1 or PKM2 were employed. The quantitative values obtained for PKM1 and PKM2 were set in ratio with PKM1+2 and all samples were corrected accordingly.

Pyruvate kinase (PK) activity

PK was assessed using the Pyruvate Kinase Activity Assay Kit (MAK072, Sigma), according to the manufacture`s instruction. Briefly, cells were rapidly homogenized and the rate of PK activity was measured by assessing the fluorescence intensity every 5 minutes until the value of the most active sample was higher than the one of the highest standard. The results were then reported to the total number of cells calculated according to the BCA protein assay kit (23225, Pierce, Thermo Scientific). Both PK and protein measurements were obtained with a Tecan reader (InfiniteM200).

Bioenergetic profiling

Assessment of cellular energy metabolism was performed using Seahorse XF24 extra-cellular flux analyzer (Seahorse Bioscience, www.seahorsebio.com), as previously described [31]. The instrument allows the simultaneous quantification of mitochondrial respiration (oxygen consumption rate, OCR) and glycolysis to lactic acid (extracellular acidification rate, ECAR). Four mitochondrial inhibitors (all from Sigma) were used in succession. After three basal measurements, 1μM oligomycin, a complex V blocker, was added to inhibit OXPHOS. After time point 6, the uncoupling agent FCCP was injected into the wells leading to the collapse of the mitochondrial membrane potential and to the consumption of oxygen in the absence of ATP production. The same FCCP concentration (1μM) was added again after time point 9 to monitor the continuous mitochondrial uncoupling. Finally, 1μM rotenone (complex I blocker) and 1μM antimycin A (complex III blocker) were simultaneously injected to completely inhibit mitochondrial respiration, thus enabling the calculations of both mitochondrial and non-mitochondrial respiratory fractions. 40,000 fibroblasts were plated into each well of the XF-24 well plates approximately 18h before the analysis. Assays were initiated by removing the growth medium and replacing it with unbuffered media, prepared as previously described [31].

Statistical analysis

Data are expressed as mean and standard error of the mean (SEM), unless stated otherwise. Data were analyzed using GraphPad-Prism software (Prism 4.0, GraphPad Software, Inc.) and Windows XP Excel (Microsoft).

Results

HIF1α activation stimulates glycolysis and enhances the efficiency of reprogramming

We previously discovered that the protein expression level of PDK1 is elevated in human PSCs compared to somatic cells or to PSC-differentiated cells [31]. These findings have been independently demonstrated [25] and further supported by the observation that small molecule-based PDK1 induction can significantly improve cellular reprogramming [22]. Since PDK1 is a known downstream target of HIF1α [15, 16], we first sought to determine the level of HIFα protein expression in undifferentiated PSCs. In agreement with previous data obtained on hESCs [34], we verified that HIF1α and HIF2α are not constitutively activated in human PSCs (Figure 1A). The pattern of nuclear accumulation following hypoxic stimulation was a bit different for HIF1α and HIF2α, as it was comparable in both fibroblasts and PSCs for HIF1α and instead only present in PSCs for HIF2α, suggesting that HIF2α could play a more important role in undifferentiated stem cells, as previously described [47].

We then investigated whether HIF1α activation may influence the induction of pluripotency. We observed that the daily addition of 100μM of the PHD inhibitor ethyl-3,4-dihydroxybenzoate (EDHB) to BJ foreskin fibroblasts could lead to significant increase in the efficiency of reprogramming (from 0.001% in BJ cells to 0.005% in BJ cells treated with EDHB). This was assayed based on the number of hESC-like colonies expressing the pluripotency-regulating protein NANOG four weeks after retroviral transduction of the four Yamanaka factors (4F) (Figure 1B, Student's *t* test, 4F versus 4F EDHB, p=0.0063). These

findings are in agreement with a previous report showing that a different PHD inhibitor, N-oxaloylglycine, and another HIF1α inducer, Quercetin, could lead to increased efficiency of cellular reprogramming in human fibroblast cells [22]. Moreover, HIF1α over-expression has been found to improve the induction of iPSC-like colonies in the A549 cancer cell line [48].

Since we previously demonstrated that reprogramming to pluripotency is associated with a shift to glycolysis [21], we tested whether the HIF1α activator that facilitated reprogramming was capable of enhancing glycolysis. Indeed, short-term treatment with EDHB was sufficient to decrease the rate of cellular OXPHOS (Figure 1C) and increase glycolytic metabolism (Figure 1D). Several parameters related to mitochondrial respiration were strongly lowered by the treatment, including the basal respiration, the ATP turnover, the maximal respiration rate, and the spare respiratory capacity (Supp. Fig. 1). Overall EDHB significantly reduced the ratio between oxygen consumption rate (OCR) and extracellular acidification rate (ECAR) (Figure 1E, Student's *t* test, EDHB treated versus untreated, $p<0.005$), indicative of a switch to glycolysis. Hence, mimicking HIF1α stimulation in somatic cells can amplify the Warburg-like metabolic shift thereby improving iPSC generation.

HIF1α depletion down-regulates the glycolytic pathway and hampers iPSC generation

In order to establish whether the activation of the HIF1α pathway during reprogramming is critical for the generation of iPSCs rather than simply supportive, we stably knocked-down HIF1α in BJ fibroblasts (HIF1-KD) using a lentivirus-based RNA interference approach. A scrambled knockdown (SCR-KD) was included as control. Immunoblot analysis confirmed that HIF1-KD fibroblasts were incapable of accumulating HIF1α protein within the nucleus under hypoxic exposure (Figure 2A). Both HIF1-KD BJ and SCR-KD BJ exhibited normal fibroblast-like growth features and did not show signs of early senescence, as shown by β-galactosidase staining (Supp. Fig.2A).

Strikingly, NANOG-positive colonies failed to appear in HIF1-KD cells reprogrammed with the 4F retroviral transduction (Figure 2B), while SCR-KD cells retained the ability to give rise to NANOG-positive hESC-like colonies with an efficiency approximately similar to that of wild type BJ fibroblasts (around 0.001%) (Figure 2B). The addition of EDHB was not sufficient to overcome the reprogramming block in HIF1-KD cells (data not shown). In addition, we assessed the effect of HIF1α depletion using an alternative non-integrative episomal plasmid reprogramming approach [43]. Consistent with the retroviral data, wild-type BJ and SCR-KD BJ fibroblasts transfected with the episomal plasmids could generate NANOG-positive colonies with a similar efficiency (around 0.0008%) after four weeks of reprogramming (Figure 2B). However, HIF1-KD BJ fibroblasts failed to derive hESC-like colonies (Figure 2B). These results imply that cells depleted of HIF1α may be incapable of achieving a pluripotent state regardless of the reprogramming method, pointing towards an instrumental role of HIF1α in the induction of pluripotency.

We then sought to gain insights into the possible mechanisms responsible for the inability of HIF1-KD cells to undergo efficient reprogramming and performed global transcriptomics. Reassuringly, the results confirmed *HIF1A* as the most down-regulated gene in HIF1-KD BJ compared to SCR-KD BJ (Supp. Table 1). Interestingly, pathway analysis revealed that among the most significantly down-regulated pathways in HIF1-KD compared to SCR-KD (fold change > 1.5) there were the mTOR signaling pathway, which is known to be associated with HIF1α and the regulation of energy metabolism [4], and the pathways related to glycolysis and gluconeogenesis (Figure 2C). We then assessed the bioenergetic profiling of fibroblasts and found that the lack of HIF1α did not alter their basal glucose metabolism, as indicated by the maintenance of OCR/ECAR ratio (Figure 2D). Indeed, the rate of OXPHOS (Supp. Fig. 2B) and glycolysis (Supp. Fig. 2B) appeared similar in HIF1-KD fibroblasts, SCR-KD, and wild-type BJ fibroblasts. Overall, the data suggest that HIF1α ablation may not be sufficient to alter the basal metabolism of fibroblasts but it might hinder

reprogramming through the down-regulation of target genes that have to be activated in order to enable the establishment of pluripotency. Since genes associated with glycolysis and gluconeogenesis have been previously found to be up-regulated in undifferentiated PSCs compared to fibroblasts [25, 31], it may be conceivable that cells that are not capable of correctly activating a glycolytic program may also be refractory to efficient iPSC conversion.

Up-regulation of HIF1α-associated metabolic regulators during initiation of reprogramming

To follow up the hypothesis that knockdown of HIF1α may alter the transcriptional re-configuration of energy metabolism and that this may be crucial for reprogramming, we sought to focus on regulated gene expression occurring within the initiation phase of iPSC derivation. Indeed, we previously observed that the Gene Ontology (GO) biological process of "response to hypoxia" was significantly regulated during early reprogramming [40]. We thus analyzed the transcriptome of foreskin fibroblasts (FFs) at 24h, 48h, and 72h after i) treatment with 100μM EDHB (EDHB 24h, 28h, 72h), ii) transduction with the four reprogramming factors (4F 24h, 48h, 72h), and iii) both (4F EDHB 24h, 48h, 72h). These data were compared to the transcriptome of fully reprogrammed iPSCs derived from FFs [21, 31], from adult dermal fibroblasts (DFs) [38], and from amniotic fluid cells (AFCs) [44], and of hESCs.

Principal component analysis (PCA) revealed that at these early time points neither HIF1α manipulation nor 4F retroviral transduction was sufficient to extensively alter the global transcriptional signature of somatic cells, which clustered together and apart from all PSCs (Figure 3A). The expression level of the most significantly highly up- or down-regulated genes (fold change > 20) in PSCs compared to somatic cells remained unaffected in somatic fibroblasts exposed to 4F transduction and/or HIF1α activation (Figure 3B). In particular, among these top-regulated genes, none appeared regulated in EDHB-treated

fibroblasts (Supp. Table 2) and only a few genes related to the viral-mediated introduction of transcription factors (such as *OCT4*, the *OCT4* pseudogene-1, and the cancer-associated *H19*) were up-regulated in early 4F-transduced fibroblasts (Supp. Table 2).

We next focused on genes associated with HIF1α, energy metabolism, and mTOR signaling pathways (Supp. Table 3). The mRNA expression level of *HIF1A* and *HIF2A* genes was not altered upon early reprogramming or EDHB treatment (Supp. Table 3), as also confirmed by qPCR analyses (Supp. Fig. 3A). Accordingly, no changes in *HIF1A* or *HIF2A* gene expression could be observed in PSCs compared to somatic cells, both under normoxic and hypoxic exposure (Supp. Fig. 3B). This is in agreement with previous findings showing the lack of *HIF1A* transcriptional activation under hypoxia in hESCs [34]. Interestingly, however, the expression of some of the genes associated with energy metabolism underwent modifications during early reprogramming (Supp. Table 3, Supp. Fig. 4). Among the metabolism-related genes exhibiting early up-regulation in 4F-transduced cells or EDHB-treated cells, we identified three HIF1α target factors known to regulate a reconfiguration of energy flux: *PKM2, PDK1*, and *PDK3* (Supp. Fig. 4).

PKM2, PDK1, and *PDK3* gene expression in fibroblasts showed an increase following EDHB treatment, as confirmed by qPCR analysis (Figure 4A). This is in agreement with previous data linking HIF1α activation with *PDK1-3* induction [15-17] and with *PKM2* gene transcription [18]. Importantly, the sole introduction of the four factors into fibroblasts resulted in the early up-regulation of *PDK1* (Figure 4A). On the other hand, *PKM2* and *PDK3* were not up-regulated following 4F transduction (Figure 4A), indicating that the conventional Yamanaka protocol may not be sufficient to induce the early expression of these two factors which instead require the additional activation of the HIF1α pathway.

Finally, we confirmed that elevated expression of these three glycolytic regulators could occur in human fibroblasts following both EDHB treatment (Figure 4B) and hypoxic exposure (Figure 4C). Importantly, *PKM2, PDK1*, and *PDK3* were not up-regulated in HIF1-

KD fibroblasts treated with EDHB (Figure 4B, one-way ANOVA, $p<0.005$) or cultured under hypoxia (Figure 4C, one-way ANOVA, $p<0.005$). No alteration of the basal expression of genes associated with the pathways of HIF1α, energy metabolism, and mTOR could be detected in HIF1-KD compared to SCR-KD (with the exception of the down-regulation of *HIF1a*) (Supp. Table 3). Hence, although fibroblasts bearing HIF1α knockdown showed a normal fibroblast-like basal metabolism (Figure 2D) and normal fibroblast-like metabolic-related transcriptional signature (Supp. Table 3), they appeared incapable of up-regulating the expression of key glycolytic inducers. This implicates the Warburg-like transcriptional modulation of energy metabolism as a potential enabling step for initiating cellular reprogramming.

Elevated expression of the HIF1α-related glycolytic regulators PKM2, PDK1, and PDK3 in pluripotent stem cells

We next investigated the association of the three HIF1α-related metabolic regulators with pluripotency. The expression level of *PDK1*, *PDK3*, and *PKM2* was measured in FFiPSCs, DFiPSCs and hESCs, under both normoxia and 24h 1% hypoxia, and compared it to that in FFs (for FFiPSCs), DFs (for DFiPSCs), and all somatic fibroblasts (for hESCs) grown under normoxic conditions. In agreement with previous protein expression data [25, 31], the transcriptional level of *PDK1* appeared up-regulated in all PSCs (Figure 5A). However, *PDK1* induction was statistically significant in iPSCs only under hypoxic conditions (Figure 5A, Student's *t* test, hypoxic iPSCs versus normoxic fibroblasts, $p<0.05$), while both normoxic and hypoxic hESCs exhibited significant *PDK1* up-regulation (Figure 5A, Student's *t* test, normoxic/hypoxic hESCs versus normoxic fibroblasts $p<0.005$). *PDK3* was significantly up-regulated in both iPSCs (Figure 5B, Student's *t* test, normoxic/hypoxic iPSCs versus normoxic fibroblasts $p<0.05$) and hESCs (Figure 5B, Student's *t* test, normoxic/hypoxic hESCs versus normoxic fibroblasts $p<0.005$) under normoxia and hypoxia,

although it was more elevated in iPSCs under hypoxic growth (Figure 5B, Student's *t* test, hypoxic iPSCs versus normoxic fibroblasts $p<0.005$). Hence, the exposure to hypoxia led to increased up-regulation of *PDK1* and *PDK* 3 in all iPSCs but not in hESCs, which showed elevated expression of the two genes already under normoxic growth (Figure 5A and 5B). This differential response to hypoxic stimuli between somatic-derived and embryonic-derived PSCs may be explained by recent evidence demonstrating that they may not be equivalent in terms of their pluripotency [49-51]. Alternatively, it may be simply due to the known heterogeneity displayed by different PSC lines [52]. In any case, further studies are warranted to dissect this differential response to hypoxic stimuli between iPSCs and hESCs.

In order to dissect the role of PKM2 in PSCs, we first sought to employ mass spectrometry-based targeted proteomic analysis. This approach allows the quantification of the absolute amount of the two alternatively-spliced isoforms encoded by the *PKM2* gene, PKM1 and PKM2, and it was previously carried out in healthy and tumor-associated tissues [8]. Remarkably, in comparison to fibroblasts, both iPSCs and hESCs exhibited reduced PKM1 (Figure 5C, Student's *t* test, PSCs versus FFs $p<0.05$) coupled with significantly elevated amounts of PKM2 (Figure 5D, Student's *t* test, PSCs versus FFs $p<0.005$). Overall, the PKM2/PKM1 ratio appeared significantly increased in PSCs under both normoxic and hypoxic conditions (Figure 5E, Student's *t* test, normoxic/hypoxic PSCs versus normoxic/hypoxic FFs $p<0.01$). The PKM2 isoform is known to display reduced enzymatic activity [12]. Thus, we next measured the PK functionality in fibroblasts and PSCs and identified a diminished PK activity in all PSCs (Figure 5F, Student's *t* test, PSCs versus wild-type BJ, $p<0.005$). This implies that the elevated expression of PKM2 in PSCs may be functionally relevant and could contribute to the maintenance of the glycolytic phenotype of PSCs.

Taken together, undifferentiated iPSCs and hESCs express high levels of three HIF1α downstream targets, whose function mediates a Warburg-like effect by increasing the energy

flux in the upstream glycolytic branches and PPP, which may eventually lead to biomass stimulation and redox maintenance [6, 7]. Furthermore, since reprogramming efficiency is increased upon EDHB treatment (Figure 1B) or hypoxic stimulation [36], it is tempting to speculate that the elevated expression of *PKM2* and *PDK3* detected in fibroblasts exposed to EDHB or hypoxia (Figure 4B and 4C) may possibly play a role in improving the conversion to iPSCs by additional metabolic modulation towards a glycolytic state.

Metabolic remodeling during initiation of reprogramming

Finally, we asked whether the transcriptional activation of metabolic regulators during reprogramming initiation was sufficient to induce a metabolic reconfiguration. Bioenergetic profiling of fibroblasts following 4F transduction indicated that mitochondrial respiration increased over the first three days of reprogramming (Figure 6A). However, the elevation of glycolysis appeared more pronounced (Figure 6B). The additional treatment with EDHB resulted in enhanced glycolytic conversion, with drastic OCR reduction (Figure 6C) and higher ECAR values (Figure 6D). Overall, 4F transduction led to progressive decrease in the OCR/ECAR ratio, indicative of initial conversion to glycolytic metabolism (Figure 6E, Student's *t* test, 4F-transduced BJ versus wild-type BJ, $p<0.05$). In accordance, the amount of extracellular lactate in 4F-tranduced fibroblasts showed a similar gradual increase during the first days of reprogramming (Figure 6F, Student's *t* test, 4F-transduced BJ versus wild-type BJ, $p<0.05$). Nonetheless, this metabolic remodeling does not appear to be completed at these early stages, as shown by the much higher lactate secretion occurring in fully reprogrammed iPSCs and hESCs (Figure 6F, Student's *t* test, PSCs versus BJ, $p<0.005$). The additional exposure to a drug mimicking HIF1α activation may thus improve the efficiency of iPSC generation through the early enhancement of glycolytic activation, as shown by a dramatic OCR/ECAR decrease (Figure 6E, Student's *t* test, 4F-EDHB treated BJ versus BJ, $p<0.005$).

On the basis of data herein presented, we suggest that the introduction of the four Yamanaka factors in human fibroblasts may be sufficient to up-regulate the HIF1α target PDK1, which can in turn initiate a glycolytic program. On the other hand, the inclusion of hypoxia or EDHB treatment may stimulate the expression of additional HIF1α-related metabolic regulators PDK3 and PKM2, enhancing the glycolyitc shift at the very early stages of reprogramming and eventually leading to improved iPSC derivation. Finally, reprogramming may be inhibited in cells that are incapable of activating HIF1α and up-regulating these three metabolic regulators, further underlying the importance of HIF1α-associated metabolic restructuring in the induction of pluripotency in somatic cells (Figure 7).

Discussion

We and others have previously demonstrated that cell fate reprogramming is associated with a transition from respiratory to glycolytic metabolism [21-26]. Tumor cells are believed to undergo similar metabolic transformation events in order to sustain the cost of anabolic reactions caused by their high proliferative rate and resistance to stress signals [4]. Thus, metabolic adaptation appears as a crucial mechanism for proliferating cells, which require to build biomass and the same time preserve the redox balance [6]. Here, we sought to uncover possible mechanistic pathways underlying the metabolic reprogramming of iPSCs and demonstrated that HIF1α, a master regulator of glucose metabolism [13, 14], plays a critical role during the induction of pluripotency by modulating the early establishment of a glycolytic program.

Hypoxia and HIF1α have been previously implicated in the maintenance of pluripotency. Indeed, hypoxic conditions have been found to lead to improved stemness and reprogramming [33, 36]. HIF1α activation could induce hESC-like signature in cancer cell lines [48] and drive mouse ESCs to acquire glycolytic features upon transition towards an epiblast stem cell (EpiSC)-like state [53]. Moreover, stabilization of hypoxia and HIF1α

inhibits the metabolic shift to OXPHOS that is required for efficient differentiation of human mesenchymal stem cells [54]. Hypoxic exposure may also increase the protein expression UCP2 [55], a regulator of energy metabolism in undifferentiated PSCs [26]. Finally, hypoxia might lead to OCT4 reactivation to promote the de-differentiation of PSC-derived progenies [56]. Our results provide additional support for all these findings and demonstrate that cells incapable of activating a HIF1α response might also be refractory to reprogramming, thus underlying the critical importance of this pathway for the induction and maintenance of pluripotency.

Our data suggest that a glycolytic shift may be instrumental for reprogramming as it may be set into motion during the reprogramming initiation stage through the early up-regulation of the HIF1α target PDK1. Indeed, PSCs exhibit elevated PDK1 protein expression [25, 31]. Moreover, small molecule-based activation of PDK1 can improve iPSC derivation [22], while PDK1 inhibitors lead to reduced hESC-like colony formation [23]. Hence, PDK1 may possibly represent an early marker of reprogramming involved in the Warburg-like metabolic restructuring associated with the conversion to pluripotency.

The findings also provide additional support to previous data showing that during reprogramming, glycolysis-associated genes may be up-regulated prior to genes involved in self-renewal and pluripotency [23]. Furthermore, transcriptional changes in the processes related to cellular metabolism have been detected during the first initial wave of reprogramming, which has been suggested to be under the control of KLF4 and c-MYC [57]. It is thus tempting to speculate that KLF4 and c-MYC may be driving the transcriptional and bioenergetic modulation observed during the initiation of cellular reprogramming. Indeed, the oncogene c-MYC can co-operate with HIF1α to induce a transcriptional program leading to stimulated glycolytic activity [58, 59], although a glycolytic shift has been observed even in iPSCs derived in the absence of c-MYC [23]. KLF4 may be capable of activating glycolytic metabolism in cancer cells [60] and KLF5, which can substitute KLF4 in the reprogramming

cocktail [61], can regulate energy metabolism and up-regulates uncoupling protein 2 (UCP2) [62], a protein recently linked to the glycolytic state of PSCs [26]. Nonetheless, it may as well be that the key stemness factor OCT4 could regulate downstream targets implicated in OXPHOS and glycolysis [28, 63]. In fact, OCT4 expression intermingles with HIF signaling pathways [47] and may positively interact with PKM2 [64]. Further studies are warranted to clearly dissect the specific roles of the Yamanaka factors in the remodeling of energy metabolism of reprogrammed cells.

Finally, since reconfiguration of glucose metabolism could have significant advantages in preventing redox imbalance [5, 65], it is conceivable that iPSC generation may require such metabolic reprogramming in order to safeguard the genome integrity. Nuclear and mitochondrial genetic defects have been reported in human iPSCs [31, 66, 67]. Perhaps, the suppression of metabolic resetting may function as a reprogramming roadblock by inducing an uncontrolled rise of genomic damage which may be incompatible with continuous cell growth. In accordance, pro-oxidant reactions can promote PSC differentiation [68].

It is important to note that our analyses were performed on whole cultures and may thus not necessarily mirror the situation occurring in the small percentage of cells actually undergoing reprogramming. Reassuringly, a recent work employing single-cell analysis showed that reprogramming is initiated in the majority of virally transduced fibroblasts, although only completed in a smaller cellular subpopulation [69]. Since we mainly focused on early reprogramming initiation, it is then possible that our data may reflect real reprogramming-related cellular conditions. Nevertheless, given the known heterogeneity of single PSC lines [49, 52], it would be of interest to repeat our relatively small-scale investigation (which included two hESC lines and thirteen human iPSC lines derived from three different cell sources, i.e. foreskin fibroblasts, dermal fibroblasts, and amniotic fluid

cells) using larger datasets of several human and murine PSCs to clearly demonstrate the role of HIF1α and glycolytic regulation in cell fate conversion.

Overall, our results indicate that HIF1α-mediated reconfiguration of glucose metabolism may represent an early enabling step of cellular reprogramming, a barrier that has to be overcome in order to make somatic cells capable of sustaining their newly acquired proliferative and biosynthetic needs. We anticipate that the study of metabolism in stem cells may unveil critical mechanisms governing the induction of pluripotency, eventually elucidating the pathways responsible for allowing this remarkable example of cellular plasticity.

Acknowledgements

The authors would like to thank Beata Lukaszewska for help in the PKM quantification and Claudia Vogelgesang and Aydah Sabah at the microarray facility. The authors declare no competing financial or commercial interests and acknowledge support from the Max Planck Society. A.P. acknowledges support from the Fritz Thyssen Foundation (grant AZ. 10.11.2.160). M.R. is a Wellcome Trust Research Career Development and Wellcome-Beit fellow. J.A. acknowledges support from the German Federal Ministry of Education and Research (BMBF) grants (01GN1005), (01GN0807) and (0315717A), which is a partner of the ERASysBio+ initiative supported under the EU ERA-NET Plus scheme in FP7.

References

1. Semenza, G.L., *Life with oxygen.* Science, 2007. **318**(5847): p. 62-4.
2. Warburg, O., *On the origin of cancer cells.* Science, 1956. **123**(3191): p. 309-14.
3. Koppenol, W.H., Bounds, P.L., and Dang, C.V., *Otto Warburg's contributions to current concepts of cancer metabolism.* Nat Rev Cancer, 2011. **11**(5): p. 325-37.
4. Levine, A.J. and Puzio-Kuter, A.M., *The control of the metabolic switch in cancers by oncogenes and tumor suppressor genes.* Science, 2010. **330**(6009): p. 1340-4.
5. Cairns, R.A., Harris, I.S., and Mak, T.W., *Regulation of cancer cell metabolism.* Nat Rev Cancer, 2011. **11**(2): p. 85-95.

6. Vander Heiden, M.G., Cantley, L.C., and Thompson, C.B., *Understanding the Warburg effect: the metabolic requirements of cell proliferation.* Science, 2009. **324**(5930): p. 1029-33.
7. Ralser, M., Wamelink, M.M., Kowald, A., Gerisch, B., Heeren, G., Struys, E.A., Klipp, E., Jakobs, C., Breitenbach, M., Lehrach, H., and Krobitsch, S., *Dynamic rerouting of the carbohydrate flux is key to counteracting oxidative stress.* J Biol, 2007. **6**(4): p. 10.
8. Bluemlein, K., Gruning, N.M., Feichtinger, R.G., Lehrach, H., Kofler, B., and Ralser, M., *No evidence for a shift in pyruvate kinase PKM1 to PKM2 expression during tumorigenesis.* Oncotarget, 2011. **2**(5): p. 393-400.
9. Christofk, H.R., Vander Heiden, M.G., Harris, M.H., Ramanathan, A., Gerszten, R.E., Wei, R., Fleming, M.D., Schreiber, S.L., and Cantley, L.C., *The M2 splice isoform of pyruvate kinase is important for cancer metabolism and tumour growth.* Nature, 2008. **452**(7184): p. 230-3.
10. Anastasiou, D., Poulogiannis, G., Asara, J.M., Boxer, M.B., Jiang, J.K., Shen, M., Bellinger, G., Sasaki, A.T., Locasale, J.W., Auld, D.S., Thomas, C.J., Vander Heiden, M.G., and Cantley, L.C., *Inhibition of pyruvate kinase M2 by reactive oxygen species contributes to cellular antioxidant responses.* Science, 2011. **334**(6060): p. 1278-83.
11. Gruning, N.M., Rinnerthaler, M., Bluemlein, K., Mulleder, M., Wamelink, M.M., Lehrach, H., Jakobs, C., Breitenbach, M., and Ralser, M., *Pyruvate kinase triggers a metabolic feedback loop that controls redox metabolism in respiring cells.* Cell Metab, 2011. **14**(3): p. 415-27.
12. Chaneton, B. and Gottlieb, E., *Rocking cell metabolism: revised functions of the key glycolytic regulator PKM2 in cancer.* Trends Biochem Sci, 2012. **37**(8): p. 309-16.
13. Semenza, G.L., *Hypoxia-inducible factors in physiology and medicine.* Cell, 2012. **148**(3): p. 399-408.
14. Rohwer, N., Zasada, C., Kempa, S., and Cramer, T., *The growing complexity of HIF-1alpha's role in tumorigenesis: DNA repair and beyond.* Oncogene, 2013. **32**(31): p. 3569-76
15. Kim, J.W., Tchernyshyov, I., Semenza, G.L., and Dang, C.V., *HIF-1-mediated expression of pyruvate dehydrogenase kinase: a metabolic switch required for cellular adaptation to hypoxia.* Cell Metab, 2006. **3**(3): p. 177-85.
16. Papandreou, I., Cairns, R.A., Fontana, L., Lim, A.L., and Denko, N.C., *HIF-1 mediates adaptation to hypoxia by actively downregulating mitochondrial oxygen consumption.* Cell Metab, 2006. **3**(3): p. 187-97.
17. Lu, C.W., Lin, S.C., Chen, K.F., Lai, Y.Y., and Tsai, S.J., *Induction of pyruvate dehydrogenase kinase-3 by hypoxia-inducible factor-1 promotes metabolic switch and drug resistance.* J Biol Chem, 2008. **283**(42): p. 28106-14.
18. Luo, W., Hu, H., Chang, R., Zhong, J., Knabel, M., O'Meally, R., Cole, R.N., Pandey, A., and Semenza, G.L., *Pyruvate kinase M2 is a PHD3-stimulated coactivator for hypoxia-inducible factor 1.* Cell, 2011. **145**(5): p. 732-44.
19. Takahashi, K. and Yamanaka, S., *Induction of pluripotent stem cells from mouse embryonic and adult fibroblast cultures by defined factors.* Cell, 2006. **126**(4): p. 663-76.
20. Ruiz, S., Panopoulos, A.D., Herrerias, A., Bissig, K.D., Lutz, M., Berggren, W.T., Verma, I.M., and Izpisua Belmonte, J.C., *A High Proliferation Rate Is Required for Cell Reprogramming and Maintenance of Human Embryonic Stem Cell Identity.* Curr Biol, 2010.
21. Prigione, A., Fauler, B., Lurz, R., Lehrach, H., and Adjaye, J., *The senescence-related mitochondrial/oxidative stress pathway is repressed in human induced pluripotent stem cells.* Stem Cells, 2010. **28**(4): p. 721-33.

22. Zhu, S., Li, W., Zhou, H., Wei, W., Ambasudhan, R., Lin, T., Kim, J., Zhang, K., and Ding, S., *Reprogramming of human primary somatic cells by OCT4 and chemical compounds.* Cell Stem Cell, 2010. **7**(6): p. 651-5.
23. Folmes, C.D., Nelson, T.J., Martinez-Fernandez, A., Arrell, D.K., Lindor, J.Z., Dzeja, P.P., Ikeda, Y., Perez-Terzic, C., and Terzic, A., *Somatic oxidative bioenergetics transitions into pluripotency-dependent glycolysis to facilitate nuclear reprogramming.* Cell Metab, 2011. **14**(2): p. 264-71.
24. Panopoulos, A.D., Yanes, O., Ruiz, S., Kida, Y.S., Diep, D., Tautenhahn, R., Herrerias, A., Batchelder, E.M., Plongthongkum, N., Lutz, M., Berggren, W.T., Zhang, K., Evans, R.M., Siuzdak, G., and Belmonte, J.C., *The metabolome of induced pluripotent stem cells reveals metabolic changes occurring in somatic cell reprogramming.* Cell Res, 2011. **22**(1): p. 168-77.
25. Varum, S., Rodrigues, A.S., Moura, M.B., Momcilovic, O., Easley, C.A.t., Ramalho-Santos, J., Van Houten, B., and Schatten, G., *Energy metabolism in human pluripotent stem cells and their differentiated counterparts.* PLoS One, 2011. **6**(6): p. e20914.
26. Zhang, J., Khvorostov, I., Hong, J.S., Oktay, Y., Vergnes, L., Nuebel, E., Wahjudi, P.N., Setoguchi, K., Wang, G., Do, A., Jung, H.J., McCaffery, J.M., Kurland, I.J., Reue, K., Lee, W.N., Koehler, C.M., and Teitell, M.A., *UCP2 regulates energy metabolism and differentiation potential of human pluripotent stem cells.* EMBO J, 2011. **30**(24): p. 4860-73.
27. Zhang, J., Nuebel, E., Daley, G.Q., Koehler, C.M., and Teitell, M.A., *Metabolic Regulation in Pluripotent Stem Cells during Reprogramming and Self-Renewal.* Cell Stem Cell, 2012. **11**(5): p. 589-95.
28. Folmes, C.D., Dzeja, P.P., Nelson, T.J., and Terzic, A., *Metabolic plasticity in stem cell homeostasis and differentiation.* Cell Stem Cell, 2012. **11**(5): p. 596-606.
29. Xu, X., Duan, S., Yi, F., Ocampo, A., Liu, G.H., and Izpisua Belmonte, J.C., *Mitochondrial Regulation in Pluripotent Stem Cells.* Cell Metab, 2013.
30. Bukowiecki, R., Adjaye, J., and Prigione, A., *Mitochondrial function in pluripotent stem cells and cellular reprogramming.* Gerontology, 2013.
31. Prigione, A., Lichtner, B., Kuhl, H., Struys, E.A., Wamelink, M., Lehrach, H., Ralser, M., Timmermann, B., and Adjaye, J., *Human induced pluripotent stem cells harbor homoplasmic and heteroplasmic mitochondrial DNA mutations while maintaining human embryonic stem cell-like metabolic reprogramming.* Stem Cells, 2011. **29**(9): p. 1338-48.
32. Armstrong, L., Tilgner, K., Saretzki, G., Atkinson, S.P., Stojkovic, M., Moreno, R., Przyborski, S., and Lako, M., *Human induced pluripotent stem cell lines show stress defense mechanisms and mitochondrial regulation similar to those of human embryonic stem cells.* Stem Cells, 2010. **28**(4): p. 661-73.
33. Ezashi, T., Das, P., and Roberts, R.M., *Low O2 tensions and the prevention of differentiation of hES cells.* Proc Natl Acad Sci U S A, 2005. **102**(13): p. 4783-8.
34. Forristal, C.E., Wright, K.L., Hanley, N.A., Oreffo, R.O., and Houghton, F.D., *Hypoxia inducible factors regulate pluripotency and proliferation in human embryonic stem cells cultured at reduced oxygen tensions.* Reproduction, 2010. **139**(1): p. 85-97.
35. Mohyeldin, A., Garzon-Muvdi, T., and Quinones-Hinojosa, A., *Oxygen in stem cell biology: a critical component of the stem cell niche.* Cell Stem Cell, 2010. **7**(2): p. 150-61.
36. Yoshida, Y., Takahashi, K., Okita, K., Ichisaka, T., and Yamanaka, S., *Hypoxia enhances the generation of induced pluripotent stem cells.* Cell Stem Cell, 2009. **5**(3): p. 237-41.

37. Lengner, C.J., Gimelbrant, A.A., Erwin, J.A., Cheng, A.W., Guenther, M.G., Welstead, G.G., Alagappan, R., Frampton, G.M., Xu, P., Muffat, J., Santagata, S., Powers, D., Barrett, C.B., Young, R.A., Lee, J.T., Jaenisch, R., and Mitalipova, M., *Derivation of pre-X inactivation human embryonic stem cells under physiological oxygen concentrations.* Cell, 2010. **141**(5): p. 872-83.
38. Prigione, A., Hossini, A.M., Lichtner, B., Serin, A., Fauler, B., Megges, M., Lurz, R., Lehrach, H., Makrantonaki, E., Zouboulis, C.C., and Adjaye, J., *Mitochondrial-associated cell death mechanisms are reset to an embryonic-like state in aged donor-derived iPS cells harboring chromosomal aberrations.* PLoS One, 2011. **6**(11): p. e27352.
39. Warnecke, C., Griethe, W., Weidemann, A., Jurgensen, J.S., Willam, C., Bachmann, S., Ivashchenko, Y., Wagner, I., Frei, U., Wiesener, M., and Eckardt, K.U., *Activation of the hypoxia-inducible factor-pathway and stimulation of angiogenesis by application of prolyl hydroxylase inhibitors.* FASEB J, 2003. **17**(9): p. 1186-8.
40. Mah, N., Wang, Y., Liao, M.C., Prigione, A., Jozefczuk, J., Lichtner, B., Wolfrum, K., Haltmeier, M., Flottmann, M., Schaefer, M., Hahn, A., Mrowka, R., Klipp, E., Andrade-Navarro, M.A., and Adjaye, J., *Molecular insights into reprogramming-initiation events mediated by the OSKM gene regulatory network.* PLoS One, 2011. **6**(8): p. e24351.
41. Sowter, H.M., Raval, R.R., Moore, J.W., Ratcliffe, P.J., and Harris, A.L., *Predominant role of hypoxia-inducible transcription factor (Hif)-1alpha versus Hif-2alpha in regulation of the transcriptional response to hypoxia.* Cancer Res, 2003. **63**(19): p. 6130-4.
42. Leurs, C., Jansen, M., Pollok, K.E., Heinkelein, M., Schmidt, M., Wissler, M., Lindemann, D., Von Kalle, C., Rethwilm, A., Williams, D.A., and Hanenberg, H., *Comparison of three retroviral vector systems for transduction of nonobese diabetic/severe combined immunodeficiency mice repopulating human CD34+ cord blood cells.* Hum Gene Ther, 2003. **14**(6): p. 509-19.
43. Yu, J., Chau, K.F., Vodyanik, M.A., Jiang, J., and Jiang, Y., *Efficient feeder-free episomal reprogramming with small molecules.* PLoS One, 2011. **6**(3): p. e17557.
44. Wolfrum, K., Wang, Y., Prigione, A., Sperling, K., Lehrach, H., and Adjaye, J., *The LARGE Principle of Cellular Reprogramming: Lost, Acquired and Retained Gene Expression in Foreskin and Amniotic Fluid-Derived Human iPS Cells.* PLoS One, 2010. **5**(10).
45. Kawamura, T., Suzuki, J., Wang, Y.V., Menendez, S., Morera, L.B., Raya, A., Wahl, G.M., and Izpisua Belmonte, J.C., *Linking the p53 tumour suppressor pathway to somatic cell reprogramming.* Nature, 2009. **460**(7259): p. 1140-4.
46. Rohwer, N., Welzel, M., Daskalow, K., Pfander, D., Wiedenmann, B., Detjen, K., and Cramer, T., *Hypoxia-inducible factor 1alpha mediates anoikis resistance via suppression of alpha5 integrin.* Cancer Res, 2008. **68**(24): p. 10113-20.
47. Covello, K.L., Kehler, J., Yu, H., Gordan, J.D., Arsham, A.M., Hu, C.J., Labosky, P.A., Simon, M.C., and Keith, B., *HIF-2alpha regulates Oct-4: effects of hypoxia on stem cell function, embryonic development, and tumor growth.* Genes Dev, 2006. **20**(5): p. 557-70.
48. Mathieu, J., Zhang, Z., Zhou, W., Wang, A.J., Heddleston, J.M., Pinna, C.M., Hubaud, A., Stadler, B., Choi, M., Bar, M., Tewari, M., Liu, A., Vessella, R., Rostomily, R., Born, D., Horwitz, M., Ware, C., Blau, C.A., Cleary, M.A., Rich, J.N., and Ruohola-Baker, H., *HIF induces human embryonic stem cell markers in cancer cells.* Cancer Res, 2011. **71**(13): p. 4640-52.
49. Yamanaka, S., *Induced pluripotent stem cells: past, present, and future.* Cell Stem Cell, 2012. **10**(6): p. 678-84.

50. Ohi, Y., Qin, H., Hong, C., Blouin, L., Polo, J.M., Guo, T., Qi, Z., Downey, S.L., Manos, P.D., Rossi, D.J., Yu, J., Hebrok, M., Hochedlinger, K., Costello, J.F., Song, J.S., and Ramalho-Santos, M., *Incomplete DNA methylation underlies a transcriptional memory of somatic cells in human iPS cells.* Nat Cell Biol, 2011. **13**(5): p. 541-9.
51. Kim, K., Zhao, R., Doi, A., Ng, K., Unternaehrer, J., Cahan, P., Huo, H., Loh, Y.H., Aryee, M.J., Lensch, M.W., Li, H., Collins, J.J., Feinberg, A.P., and Daley, G.Q., *Donor cell type can influence the epigenome and differentiation potential of human induced pluripotent stem cells.* Nat Biotechnol, 2011. **29**(12): p. 1117-9.
52. Cahan, P. and Daley, G.Q., *Origins and implications of pluripotent stem cell variability and heterogeneity.* Nat Rev Mol Cell Biol, 2013. **14**(6): p. 357-68.
53. Zhou, W., Choi, M., Margineantu, D., Margaretha, L., Hesson, J., Cavanaugh, C., Blau, C.A., Horwitz, M.S., Hockenbery, D., Ware, C., and Ruohola-Baker, H., *HIF1alpha induced switch from bivalent to exclusively glycolytic metabolism during ESC-to-EpiSC/hESC transition.* EMBO J, 2012. **31**(9): p. 2103-16.
54. Hsu, S.H., Chen, C.T., and Wei, Y.H., *Inhibitory Effects of Hypoxia on Metabolic Switch and Osteogenic Differentiation of Human Mesenchymal Stem Cells.* Stem Cells, 2013.
55. Deng, S., Yang, Y., Han, Y., Li, X., Wang, X., Zhang, Z., and Wang, Y., *UCP2 inhibits ROS-mediated apoptosis in A549 under hypoxic conditions.* PLoS One, 2012. **7**(1): p. e30714.
56. Mathieu, J., Zhang, Z., Nelson, A., Lamba, D.A., Reh, T.A., Ware, C., and Ruohola-Baker, H., *Hypoxia Induces Re-Entry of Committed Cells into Pluripotency.* Stem Cells, 2013.
57. Polo, J.M., Anderssen, E., Walsh, R.M., Schwarz, B.A., Nefzger, C.M., Lim, S.M., Borkent, M., Apostolou, E., Alaei, S., Cloutier, J., Bar-Nur, O., Cheloufi, S., Stadtfeld, M., Figueroa, M.E., Robinton, D., Natesan, S., Melnick, A., Zhu, J., Ramaswamy, S., and Hochedlinger, K., *A molecular roadmap of reprogramming somatic cells into iPS cells.* Cell, 2012. **151**(7): p. 1617-32.
58. Dang, C.V., Le, A., and Gao, P., *MYC-induced cancer cell energy metabolism and therapeutic opportunities.* Clin Cancer Res, 2009. **15**(21): p. 6479-83.
59. Shim, H., Dolde, C., Lewis, B.C., Wu, C.S., Dang, G., Jungmann, R.A., Dalla-Favera, R., and Dang, C.V., *c-Myc transactivation of LDH-A: implications for tumor metabolism and growth.* Proc Natl Acad Sci U S A, 1997. **94**(13): p. 6658-63.
60. Moon, J.S., Kim, H.E., Koh, E., Park, S.H., Jin, W.J., Park, B.W., Park, S.W., and Kim, K.S., *Kruppel-like factor 4 (KLF4) activates the transcription of the gene for the platelet isoform of phosphofructokinase (PFKP) in breast cancer.* J Biol Chem, 2011. **286**(27): p. 23808-16.
61. Nakagawa, M., Koyanagi, M., Tanabe, K., Takahashi, K., Ichisaka, T., Aoi, T., Okita, K., Mochiduki, Y., Takizawa, N., and Yamanaka, S., *Generation of induced pluripotent stem cells without Myc from mouse and human fibroblasts.* Nat Biotechnol, 2008. **26**(1): p. 101-6.
62. Oishi, Y., Manabe, I., Tobe, K., Ohsugi, M., Kubota, T., Fujiu, K., Maemura, K., Kubota, N., Kadowaki, T., and Nagai, R., *SUMOylation of Kruppel-like transcription factor 5 acts as a molecular switch in transcriptional programs of lipid metabolism involving PPAR-delta.* Nat Med, 2008. **14**(6): p. 656-66.
63. Chen, X., Xu, H., Yuan, P., Fang, F., Huss, M., Vega, V.B., Wong, E., Orlov, Y.L., Zhang, W., Jiang, J., Loh, Y.H., Yeo, H.C., Yeo, Z.X., Narang, V., Govindarajan, K.R., Leong, B., Shahab, A., Ruan, Y., Bourque, G., Sung, W.K., Clarke, N.D., Wei, C.L., and Ng, H.H., *Integration of external signaling pathways with the core transcriptional network in embryonic stem cells.* Cell, 2008. **133**(6): p. 1106-17.

64. Lee, J., Kim, H.K., Han, Y.M., and Kim, J., *Pyruvate kinase isozyme type M2 (PKM2) interacts and cooperates with Oct-4 in regulating transcription.* Int J Biochem Cell Biol, 2008. **40**(5): p. 1043-54.
65. Gruning, N.M. and Ralser, M., *Cancer: Sacrifice for survival.* Nature, 2011. **480**(7376): p. 190-1.
66. Gore, A., Li, Z., Fung, H.L., Young, J.E., Agarwal, S., Antosiewicz-Bourget, J., Canto, I., Giorgetti, A., Israel, M.A., Kiskinis, E., Lee, J.H., Loh, Y.H., Manos, P.D., Montserrat, N., Panopoulos, A.D., Ruiz, S., Wilbert, M.L., Yu, J., Kirkness, E.F., Izpisua Belmonte, J.C., Rossi, D.J., Thomson, J.A., Eggan, K., Daley, G.Q., Goldstein, L.S., and Zhang, K., *Somatic coding mutations in human induced pluripotent stem cells.* Nature, 2011. **471**(7336): p. 63-7.
67. Hussein, S.M., Batada, N.N., Vuoristo, S., Ching, R.W., Autio, R., Narva, E., Ng, S., Sourour, M., Hamalainen, R., Olsson, C., Lundin, K., Mikkola, M., Trokovic, R., Peitz, M., Brustle, O., Bazett-Jones, D.P., Alitalo, K., Lahesmaa, R., Nagy, A., and Otonkoski, T., *Copy number variation and selection during reprogramming to pluripotency.* Nature, 2011. **471**(7336): p. 58-62.
68. Yanes, O., Clark, J., Wong, D.M., Patti, G.J., Sanchez-Ruiz, A., Benton, H.P., Trauger, S.A., Desponts, C., Ding, S., and Siuzdak, G., *Metabolic oxidation regulates embryonic stem cell differentiation.* Nat Chem Biol, 2010. **6**(6): p. 411-7.
69. Tanabe, K., Nakamura, M., Narita, M., Takahashi, K., and Yamanaka, S., *Maturation, not initiation, is the major roadblock during reprogramming toward pluripotency from human fibroblasts.* Proc Natl Acad Sci U S A, 2013. **110**(30): p. 12172-9.

Figure legends

Figure 1. Mimicking HIF1α activation facilitates iPSC reprogramming. (A) HIF1α and HIF2α nuclear accumulation in foreskin fibroblasts (FFs), hESCs, and FFs-derived iPSCs (FFiPSCs) under normoxic conditions (N) and following 24h hypoxic incubation with 1% oxygen (H). The transcription factor YY1 was used for normalization of nuclear extracts. **(B)** BJ fibroblasts were transduced with the four factor cocktail (4F) alone or in combination with daily treatment with 100μM EDHB (4F EDHB). All cells were plated under reprogramming conditions, fixed four weeks later, and immunostained against the pluripotency-associated protein NANOG, according to the Avidin-Biotin Complex (ABC) protocol. The experiments were repeated three times. Bar graphs represent the mean and standard deviation of the average number of NANOG-positive hESC-like colonies detected. **p=0.0063, two-tailed Unpaired Student's *t* test, 4F EDHB versus 4F **(C)** Oxygen consumption rate (OCR), indicative of OXPHOS activity, was assessed using the Seahorse cellular flux analysis. Wild type FFs (BJ cells) (black line) were compared to FFs treated with EDHB for 24h (yellow line), 48h (orange line), and 72h (red line). **(D)** Extracellular acidification rate (ECAR), indicative of glycolytic activity, was measured at the same time as OCR in the same samples. **(E)** OCR/ECAR ratio was calculated in order to generate a clear estimate of the overall metabolic state of the cells. ***p<0.005, two-tailed Unpaired Student's *t* test: EDHB 24h versus BJ (p=0.0043), EDHB 48h versus BJ (p=0.0025), and EDHB 72h versus BJ (p=0.0032).

Figure 2. HIF1α knockdown inhibits reprogramming. (A) Immunoblot analysis confirmed that HIF1-KD BJ fibroblasts were incapable of accumulating HIF1α protein in the nucleus upon hypoxic stimulation while SCR-KD BJ fibroblasts retained this ability. **(B)** Wild-type BJ fibroblasts, SCR-KD BJ fibroblasts, and HIF1-KD BJ fibroblasts were reprogrammed to pluripotency using either a classical retroviral approach with the four Yamanaka factors (4F:

OCT4, SOX2, KLF4, and c-MYC) or with episomal plasmids (expressing the four factors plus NANOG, LIN28, and SV40L). After four weeks of culturing under hESC conditions, wild type BJ and SCR-KD BJ cells developed hESC-like colonies in a comparable fashion, as shown by the similar number of colonies that resulted positive for the pluripotency-associated marker NANOG (monitored with the Avidin-Biotin Complex method). However, NANOG-positive hESC-like colonies were not generated in HIF1-KD BJ cells, regardless of the reprogramming method employed. **(C)** List of the most significantly down-regulated pathways (fold change > 1.5) in HIF1-KD BJ compared to SCR-KD BJ. **(D)** The ratio of OCR/ECAR, indicating the metabolic cell state, was calculated in fibroblasts maintained under basal conditions using the seahorse bioanalyzer.

Figure 3. Transcriptional modulation during reprogramming initiation. (A) Principal component analysis (PCA) showing the clustering of the transcriptomes of the following somatic cells: FFs, DFs, amniotic fluid cells (AFCs), FFs knocked-down for HIF1α (HIF1.KD) and knocked-down for a scrambled transcript (SCR-KD), FFs transduced with the four factors only for 24, 48, and 72h (4F 24h, 4F 48h, 4F 72h) or in combination with daily 100 μM EDHB (4F EDHB 24h, 4F EDHB 48h, 4F EDHB 72h), and FFs only treated with EDHB (EDHB 24h, EDHB 48h, EDHB 72h), and the following pluripotent stem cells: hESCs, FFiPSCs, DFiPSCs, and AFCs-derived iPSCs (AFiPSCs). **(B)** Heatmap depicting the genes most highly down and up-regulated (fold change > 20) in somatic-derived and embryonic-derived pluripotent stem cells compared to wild type untreated somatic cells. Different iPSCs were compared to their respective somatic cells, while hESCs were compared to the average of all wild-type somatic cells. The samples include wild-type untreated somatic cells (grey bar), FFs harvested 24h, 48h, and 72h after 4F transduction (green bar), FFs treated with EDHB for the same time points (yellow bar), FFs exposed to both 4F and EDHB treatment (purple bar), iPSCs (black bar), and hESCs (red bar). Values indicate row-

normalized log2 average expression values; down-regulated genes are indicated in green, up-regulated genes in red.

Figure 4. Up-regulation of HIF1α-related metabolic regulators during early reprogramming. (A) qPCR analysis of HIF1α targets known to play a role in regulating glycolytic metabolism (*PKM2, PDK1*, and *PDK3*) during the first three days of reprogramming initiation. Relative mRNA level to *ACTB* is presented in comparison to wild-type untreated FFs. Green line: FFs transduced with the four factors; yellow line: FFs treated with EDHB; purple line: FFs transduced with the 4F and treated with EDHB at the same time. **(B)** Expression of *PKM2, PDK1*, and *PDK3* after 24h EDHB treatment in wild type FFs (BJ and HFF1), SCR-KD fibroblasts, and HIF1-KD fibroblasts. ***p<0.005, One-way ANOVA single factor: *PKM2* (p=5 E-07), *PDK1* (p=9 E-06), and *PDK3* (p=1 E-07). **(C)** Transcriptional level of the three glycolytic regulators after 24h exposure to 1% hypoxia. ***p<0.005, One-way ANOVA single factor: *PKM2* (p=4 E-05), *PDK1* (p=9 E-08), and *PDK3* (p=1 E-07).

Figure 5. PKM2, PDK1, and PDK3 are highly expressed in PSCs. (A) Relative *PDK1* mRNA expression in: FFiPSCs (iPS2, iPS4, iB4, and iB5) under normoxia and hypoxia in relation to normoxic FFs (HFF1 and BJ); DFiPSCs (OiPS6, OiPS8, and OiPS16) under normoxia and hypoxia in relation to normoxic DFs (NFH2); and hESCs (H1 and H9) under normoxia and hypoxia in relation to all fibroblasts (HFF1, BJ, and NFH2) grown under normoxic conditions. **p=0.0098, two-tailed Unpaired Student's *t* test, hypoxic FFiPSCs versus normoxic FFs. *p=0.043, two-tailed Unpaired Student's *t* test, hypoxic DFiPSCs versus normoxic DFs. ***p<0.005, two-tailed Unpaired Student's *t* test: normoxic hESCs versus all normoxic fibroblasts (p=0.0005), hypoxic hESCs versus all normoxic fibroblasts (p=0.0011). **(B)** Relative expression of *PDK3* in PSCs under normoxia and hypoxia compared

to normoxic somatic fibroblasts. *p=0.023, two-tailed Unpaired Student's *t* test, normoxic FFiPSCs versus normoxic FFs. **p=0.0061, two-tailed Unpaired Student's *t* test, normoxic DFiPSCs versus normoxic DFs. ***p<0.005, two-tailed Unpaired Student's *t* test: normoxic hESCs versus all normoxic fibroblasts (p=0.0007), hypoxic FFiPSCs versus normoxic FFs (p=0.0009), hypoxic DFiPSCs versus normoxic DFs (p=0.0021), hypoxic hESCs versus all normoxic fibroblasts (p=0.0002) **(C)** Absolute protein quantification of PKM1 in FFs, FFiPSCs, and hESCs. *p<0.05, two-tailed Unpaired Student's *t* test, FFiPSCs versus FFs and hESCs versus FFs. **(D)** Absolute protein quantification of PKM2 in FFs (HFF1 and BJ), FFiPSCs (iPS2, iPS4, iB4, and iB5), and hESCs (H1 and H9). ***p<0.005, two-tailed Unpaired Student's *t* test, FFiPSCs versus FFs and hESCs versus FFs. **(E)** PKM2/PKM1 ratio in FFs, FFiPSCs, and hESCs grown under normoxic and hypoxic conditions. **p<0.01, two-tailed Unpaired Student's *t* test, normoxic hESCs versus normoxic FFs. ***p<0.005, two-tailed Unpaired Student's *t* test, normoxic FFiPSCs versus normoxic FFs, hypoxic FFiPSCs versus hypoxic FFs, and hypoxic hESCs versus hypoxic FFs. **(F)** Rate of PK activity, normalized over the total protein amount, was measured in wild type FFs (BJ and HFF1), SCR-KD and HIF1-KD fibroblasts, FFiPSCs (iB4, and iB5), and hESCs (H1 and H9). ***p<0.005, two-tailed Unpaired Student's *t* test, iB4 versus BJ, iB5 versus BJ, H1 versus BJ, and H9 versus BJ.

Figure 6. Metabolic shift during early reprogramming. (A) OCR profile of wild-type FFs (BJ) and FFs after 24h, 48h, and 72h from 4F transduction. **(B)** ECAR profile of FFs at the basal level and after 4F introduction. **(C)** OCR profile in BJ fibroblasts treated with the HIF1α mimicker EDHB in addition to the 4F transduction. **(D)** ECAR profile in FFs and 4F-EDHB FFs. **(E)** OCR/ECAR ratio gradually decreases during reprogramming initiation while it is drastically reduced upon the additional introduction of EDHB to the reprogramming cocktail. *p=0.0370, two-tailed Unpaired Student's *t* test, 4F 48h versus BJ. **p=0.0062, two-tailed

Unpaired Student's *t* test, 4F 72h versus BJ. ***p<0.005, two-tailed Unpaired Student's *t* test: 4F EDHB 24h versus BJ (p=0.0045), 4F EDHB 48h versus BJ (p=0.0001), and EDHB 72h versus BJ (p=0.0002). **(F)** Production of extracellular lactate in FFs (BJ, SCR-KD, HIF1-KD), FFs transduced with the 4F, hESCs (H1 and H9), and BJ-FFiPSCs (iB4 and iB5). The values are reported to the amount of lactate generated in control wild-type BJ fibroblasts. *p<0.05, two, two-tailed Unpaired Student's *t* test: 4F 24h versus BJ (p=0.035), 4F 48h versus BJ (p=0.021). **p<0.01, two-tailed Unpaired Student's *t* test, 4F 72h versus BJ (p=0.008). ***p<0.005, two-tailed Unpaired Student's *t* test: hESCs versus BJ (p=0.0035), BJ FFiPSCs versus BJ (p=0.0041).

Figure 7. HIF1α-associated metabolic reconfiguration during reprogramming initiation. Cartoon depicting the potential mechanisms through which the introduction of the 4F or the modulation of HIF1α pathway might regulate glycolytic metabolism during the early stages of somatic cell reprogramming. The introduction of the 4F in somatic fibroblasts up-regulates the HIF1α target PDK1, which re-routes the energy flux outside the mitochondria, thereby enhancing the glycolytic metabolism. HIF1α activation up-regulates additional HIF1α targets PKM2 and PDK3, further increasing the glycolytic shift and eventually resulting in improved conversion to pluripotency.

Supp. Figure 1. (A) Basal respiration in BJ fibroblasts and in BJ fibroblasts treated for three days with 100μM EDHB was calculated by subtracting the OCR values following rotenone and antimycin A treatment from the basal OCR values. **(B)** ATP turnover was estimated by subtracting OCR measurements after oligomycin introduction from the basal OCR measurements. **(C)** Maximal respiration rate was calculated by subtracting the OCR values after rotenone and antimycin a exposure from the OCR values after FCCP exposure. **(D)**

Spare respiratory capacity was estimated by subtracting the basal OCR measurements from OCR measurements following FCCP injection.

Supp. Figure 2. (A) Neonatal foreskin fibroblasts BJ were transduced with lentiviruses containing shRNA sequences against human HIF1α (BJ-HIF1-KD) and scrambled control oligonucleotides (BJ-SCR-KD). The transduced cells maintained fibroblast-like growth features and did not display signs of senescence, as shown by lack of β-galactosidase staining. **(B)** OCR profile of BJ, SCR-KD, and HIF1-KD fibroblasts. **(C)** ECAR profile of BJ, SCR-KD, and HIF1-KD fibroblasts.

Supp. Figure 3. (A) *HIF1A* and *HIF2A* expression level in FFs following 4F transduction and/or EDHB treatment. **(B)** *HIF1A* and *HIF2A* expression level in normoxic and hypoxic FFiPSCs, DFiPSCs, and hESCs in relation to normoxic FFs, DFs, and FFs + DFs, respectively.

Supp. Figure 4. Heatmap and clustering of genes involved in energy metabolism (list taken from the Human Glucose Metabolism PCR Array). Values represent the ratio over wild-type untreated FFs; down-regulated genes are indicated in green, up-regulated genes in red. PDK1, PDK3, and PKM2 are shown with blue arrows.

Supplementary Table 1. List of the 30 most significantly down-regulated genes and 30 most significantly up-regulated genes in HIF1-KD cells compared to SCR-KD cells. Reported are the average (AVG) signals of the top genes in the two samples, the differential p values calculated between HIF1-KD and SCR-KD (light blue, $p<0.05$; dark blue, $p<0.01$), the ratios calculated as the AVG signal of HIF1-KD over the AVG signal of SCR-KD, and the log2

ratio values (fold change down-regulation >1.5 is depicted in green, fold change up-regulation >1.5 in red).

Supplementary Table 2. List of the genes most highly up- and down-regulated (fold change > 20) in PSCs compared to somatic cells. Reported are the average intensity values of all the samples utilized for global gene expression analysis. Genes up-regulated in comparison to wild-type fibroblasts are highlighted in red, down-regulated genes in green.

Supplementary Table 3. List of genes associated with HIF1α, energy metabolism, and mTOR/autophagy. Reported are the LOG2 ratio values of PSCs over the respective somatic fibroblasts (FFs for FFiPSCs, DFs for DFiPSCs, AFCs for AFiPSCs, FFs plus DFs and AFCs for hESCs), FFs transduced with the 4F or treated with EDHB over untreated wild-type FFs, and HIF1-KD BJ fibroblasts over SCR-KD BJ fibroblasts. Up-regulated genes are highlighted in red.

Supplementary Table 4. List of primers used for quantitative real-time PCR.

Figure 1

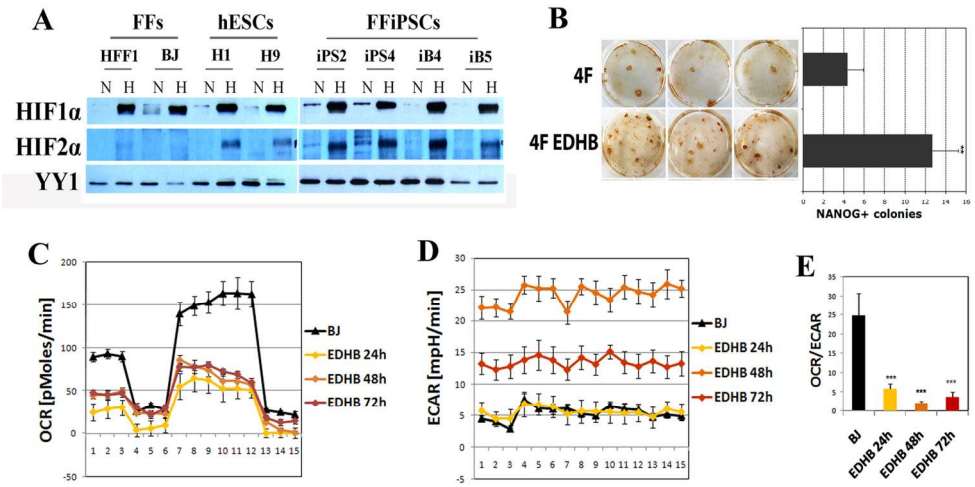

Figure 1. Mimicking HIF1α activation facilitates iPSC reprogramming. (A) HIF1α and HIF2α nuclear accumulation in foreskin fibroblasts (FFs), hESCs, and FFs-derived iPSCs (FFiPSCs) under normoxic conditions (N) and following 24h hypoxic incubation with 1% oxygen (H). The transcription factor YY1 was used for normalization of nuclear extracts. (B) BJ fibroblasts were transduced with the four factor cocktail (4F) alone or in combination with daily treatment with 100μM EDHB (4F EDHB). All cells were plated under reprogramming conditions, fixed four weeks later, and immunostained against the pluripotency-associated protein NANOG, according to the Avidin-Biotin Complex (ABC) protocol. The experiments were repeated three times. Bar graphs represent the mean and standard deviation of the average number of NANOG-positive hESC-like colonies detected. **p=0.0063, two-tailed Unpaired Student's t test, 4F EDHB versus 4F (C) Oxygen consumption rate (OCR), indicative of OXPHOS activity, was assessed using the Seahorse cellular flux analysis. Wild type FFs (BJ cells) (black line) were compared to FFs treated with EDHB for 24h (yellow line), 48h (orange line), and 72h (red line). (D) Extracellular acidification rate (ECAR), indicative of glycolytic activity, was measured at the same time as OCR in the same samples. (E) OCR/ECAR ratio was calculated in order to generate a clear estimate of the overall metabolic state of the cells. ***p<0.005, two-tailed Unpaired Student's t test: EDHB 24h versus BJ (p=0.0043), EDHB 48h versus BJ (p=0.0025), and EDHB 72h versus BJ (p=0.0032).
139x86mm (300 x 300 DPI)

Figure 2

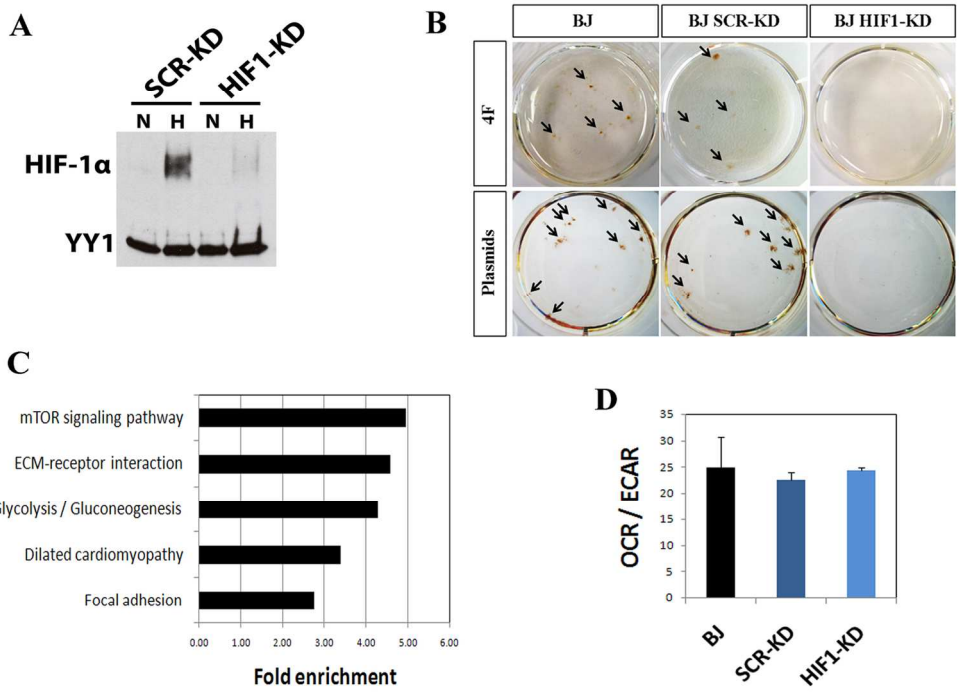

Figure 2. HIF1α knockdown inhibits reprogramming. (A) Immunoblot analysis confirmed that HIF1-KD BJ fibroblasts were incapable of accumulating HIF1α protein in the nucleus upon hypoxic stimulation while SCR-KD BJ fibroblasts retained this ability. (B) Wild-type BJ fibroblasts, SCR-KD BJ fibroblasts, and HIF1-KD BJ fibroblasts were reprogrammed to pluripotency using either a classical retroviral approach with the four Yamanaka factors (4F: OCT4, SOX2, KLF4, and c-MYC) or with episomal plasmids (expressing the four factors plus NANOG, LIN28, and SV40L). After four weeks of culturing under hESC conditions, wild type BJ and SCR-KD BJ cells developed hESC-like colonies in a comparable fashion, as shown by the similar number of colonies that resulted positive for the pluripotency-associated marker NANOG (monitored with the Avidin-Biotin Complex method). However, NANOG-positive hESC-like colonies were not generated in HIF1-KD BJ cells, regardless of the reprogramming method employed. (C) List of the most significantly down-regulated pathways (fold change > 1.5) in HIF1-KD BJ compared to SCR-KD BJ. (D) The ratio of OCR/ECAR, indicating the metabolic cell state, was calculated in fibroblasts maintained under basal conditions using the seahorse bioanalyzer.
140x114mm (300 x 300 DPI)

Figure 3

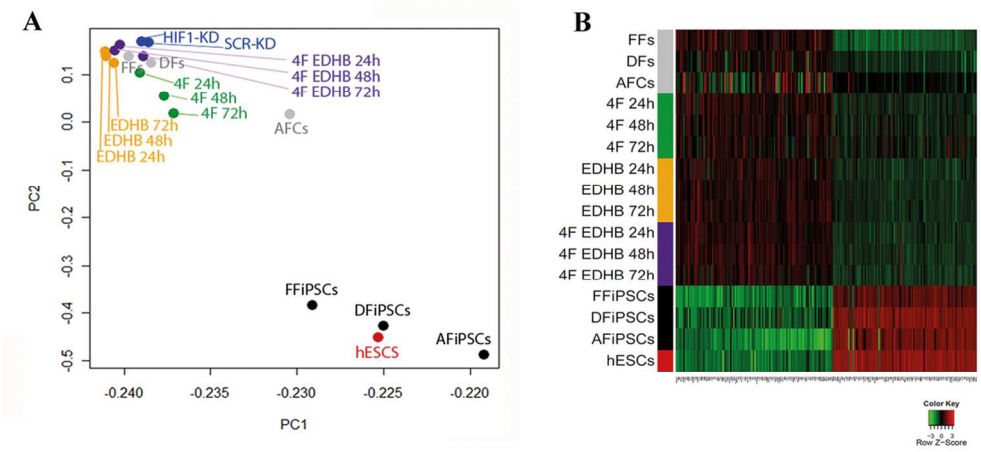

Figure 3. Transcriptional modulation during reprogramming initiation. (A) Principal component analysis (PCA) showing the clustering of the transcriptomes of the following somatic cells: FFs, DFs, amniotic fluid cells (AFCs), FFs knocked-down for HIF1α (HIF1.KD) and knocked-down for a scrambled transcript (SCR-KD), FFs transduced with the four factors only for 24, 48, and 72h (4F 24h, 4F 48h, 4F 72h) or in combination with daily 100 μM EDHB (4F EDHB 24h, 4F EDHB 48h, 4F EDHB 72h), and FFs only treated with EDHB (EDHB 24h, EDHB 48h, EDHB 72h), and the following pluripotent stem cells: hESCs, FFiPSCs, DFiPSCs, and AFCs-derived iPSCs (AFiPSCs). (B) Heatmap depicting the genes most highly down and up-regulated (fold change > 20) in somatic-derived and embryonic-derived pluripotent stem cells compared to wild type untreated somatic cells. Different iPSCs were compared to their respective somatic cells, while hESCs were compared to the average of all wild-type somatic cells. The samples include wild-type untreated somatic cells (grey bar), FFs harvested 24h, 48h, and 72h after 4F transduction (green bar), FFs treated with EDHB for the same time points (yellow bar), FFs exposed to both 4F and EDHB treatment (purple bar), iPSCs (black bar), and hESCs (red bar). Values indicate row-normalized log2 average expression values; down-regulated genes are indicated in green, up-regulated genes in red.
55x31mm (600 x 600 DPI)

Figure 4

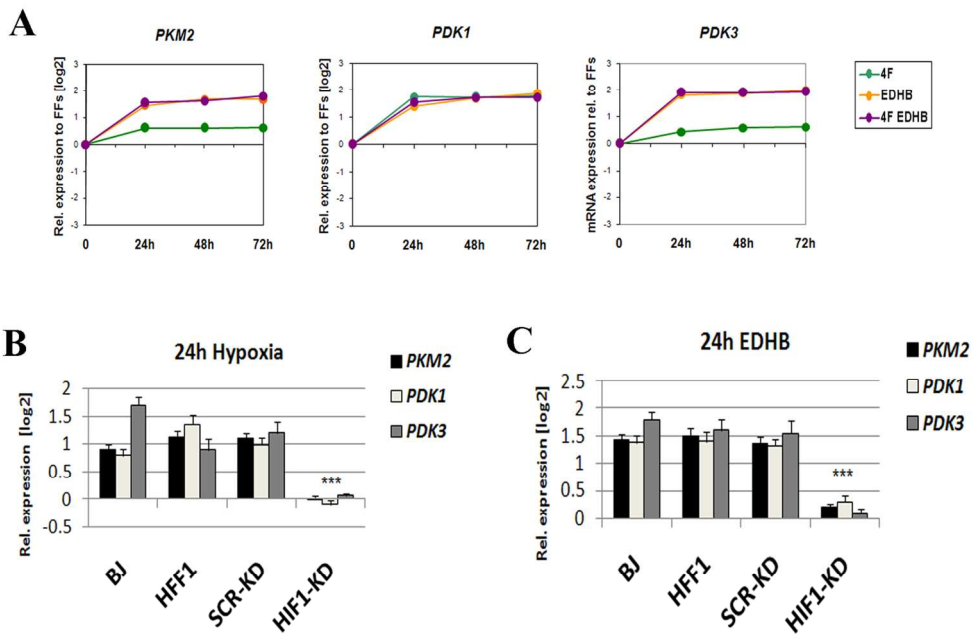

Figure 4. Up-regulation of HIF1α-related metabolic regulators during early reprogramming. (A) qPCR analysis of HIF1α targets known to play a role in regulating glycolytic metabolism (PKM2, PDK1, and PDK3) during the first three days of reprogramming initiation. Relative mRNA level to ACTB is presented in comparison to wild-type untreated FFs. Green line: FFs transduced with the four factors; yellow line: FFs treated with EDHB; purple line: FFs transduced with the 4F and treated with EDHB at the same time. (B) Expression of PKM2, PDK1, and PDK3 after 24h EDHB treatment in wild type FFs (BJ and HFF1), SCR-KD fibroblasts, and HIF1-KD fibroblasts. ***p<0.005, One-way ANOVA single factor: PKM2 (p=5 E-07), PDK1 (p=9 E-06), and PDK3 (p=1 E-07). (C) Transcriptional level of the three glycolytic regulators after 24h exposure to 1% hypoxia. ***p<0.005, One-way ANOVA single factor: PKM2 (p=4 E-05), PDK1 (p=9 E-08), and PDK3 (p=1 E-07).
77x59mm (600 x 600 DPI)

Figure 5

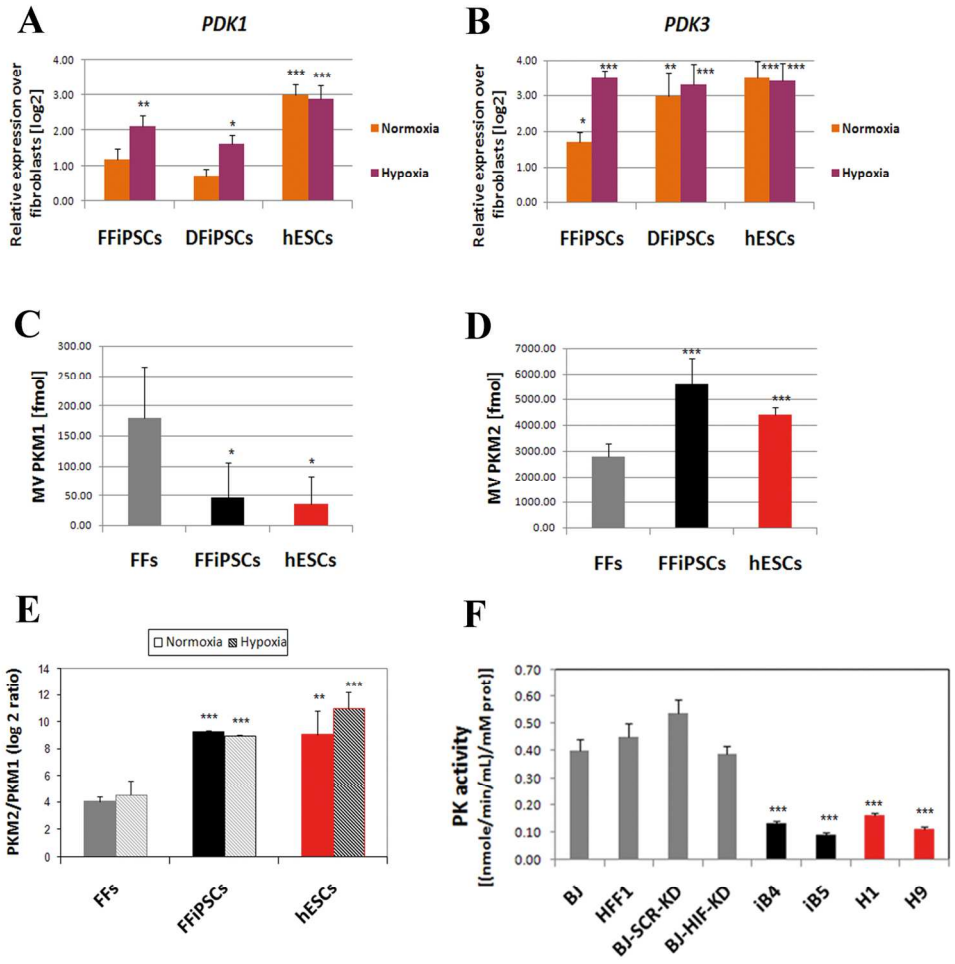

Figure 5. PKM2, PDK1, and PDK3 are highly expressed in PSCs. (A) Relative PDK1 mRNA expression in: FFiPSCs (iPS2, iPS4, iB4, and iB5) under normoxia and hypoxia in relation to normoxic FFs (HFF1 and BJ); DFiPSCs (OiPS6, OiPS8, and OiPS16) under normoxia and hypoxia in relation to normoxic DFs (NFH2); and hESCs (H1 and H9) under normoxia and hypoxia in relation to all fibroblasts (HFF1, BJ, and NFH2) grown under normoxic conditions. **p=0.0098, two-tailed Unpaired Student's t test, hypoxic FFiPSCs versus normoxic FFs. *p=0.043, two-tailed Unpaired Student's t test, hypoxic DFiPSCs versus normoxic DFs. ***p<0.005, two-tailed Unpaired Student's t test: normoxic hESCs versus all normoxic fibroblasts (p=0.0005), hypoxic hESCs versus all normoxic fibroblasts (p=0.0011). (B) Relative expression of PDK3 in PSCs under normoxia and hypoxia compared to normoxic somatic fibroblasts. *p=0.023, two-tailed Unpaired Student's t test, normoxic FFiPSCs versus normoxic FFs. **p=0.0061, two-tailed Unpaired Student's t test, normoxic DFiPSCs versus normoxic DFs. ***p<0.005, two-tailed Unpaired Student's t test: normoxic hESCs versus all normoxic fibroblasts (p=0.0007), hypoxic FFiPSCs versus normoxic FFs (p=0.0009), hypoxic DFiPSCs versus normoxic DFs (p=0.0021), hypoxic hESCs versus all normoxic fibroblasts (p=0.0002) (C) Absolute protein quantification of PKM1 in FFs, FFiPSCs, and hESCs. *p<0.05, two-tailed Unpaired Student's t test, FFiPSCs versus FFs and hESCs versus FFs. (D) Absolute protein quantification of PKM2 in FFs (HFF1 and BJ), FFiPSCs (iPS2, iPS4, iB4, and iB5), and hESCs (H1 and H9).

***p<0.005, two-tailed Unpaired Student's t test, FFiPSCs versus FFs and hESCs versus FFs. (E) PKM2/PKM1 ratio in FFs, FFiPSCs, and hESCs grown under normoxic and hypoxic conditions. **p<0.01, two-tailed Unpaired Student's t test, normoxic hESCs versus normoxic FFs. ***p<0.005, two-tailed Unpaired Student's t test, normoxic FFiPSCs versus normoxic FFs, hypoxic FFiPSCs versus hypoxic FFs, and hypoxic hESCs versus hypoxic FFs. (F) Rate of PK activity, normalized over the total protein amount, was measured in wild type FFs (BJ and HFF1), SCR-KD and HIF1-KD fibroblasts, FFiPSCs (iB4, and iB5), and hESCs (H1 and H9). ***p<0.005, two-tailed Unpaired Student's t test, iB4 versus BJ, iB5 versus BJ, H1 versus BJ, and H9 versus BJ.
80x90mm (600 x 600 DPI)

Figure 6

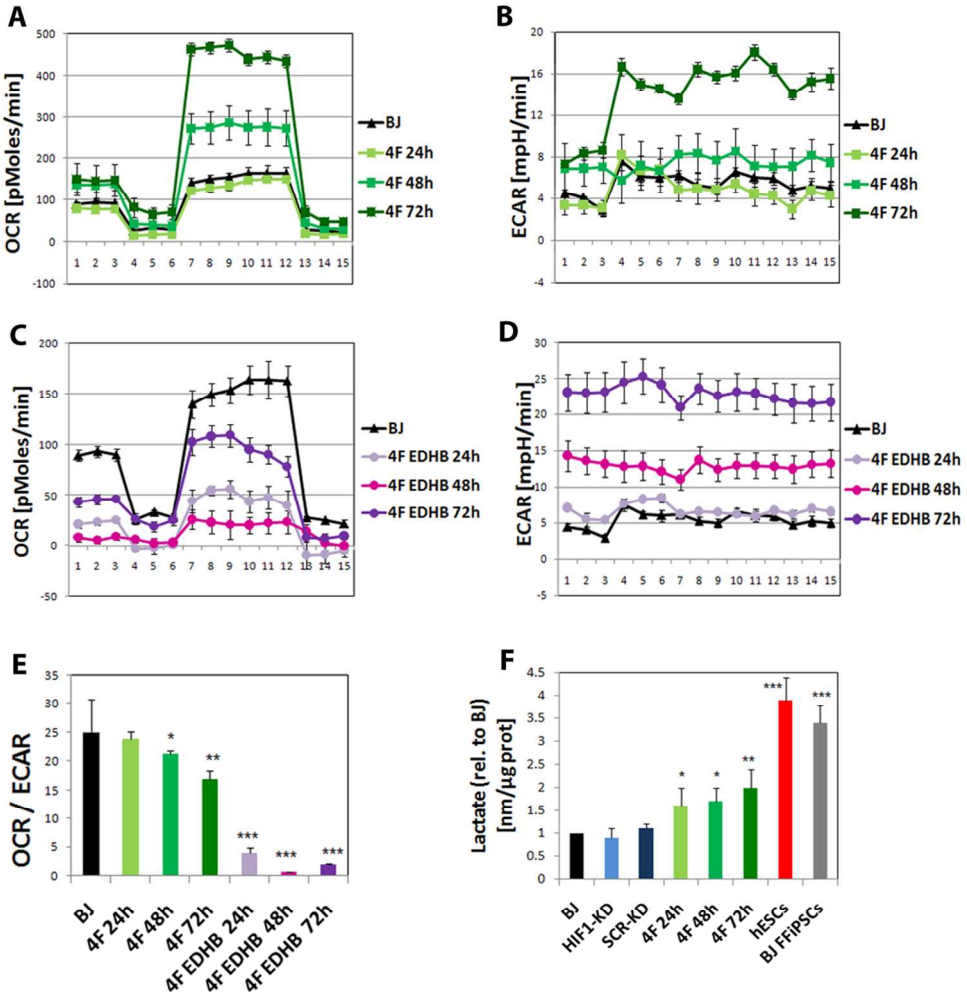

Figure 6. Metabolic shift during early reprogramming. (A) OCR profile of wild-type FFs (BJ) and FFs after 24h, 48h, and 72h from 4F transduction. (B) ECAR profile of FFs at the basal level and after 4F introduction. (C) OCR profile in BJ fibroblasts treated with the HIF1α mimicker EDHB in addition to the 4F transduction. (D) ECAR profile in FFs and 4F-EDHB FFs. (E) OCR/ECAR ratio gradually decreases during reprogramming initiation while it is drastically reduced upon the additional introduction of EDHB to the reprogramming cocktail. *p=0.0370, two-tailed Unpaired Student's t test, 4F 48h versus BJ. **p=0.0062, two-tailed Unpaired Student's t test, 4F 72h versus BJ. ***p<0.005, two-tailed Unpaired Student's t test: 4F EDHB 24h versus BJ (p=0.0045), 4F EDHB 48h versus BJ (p=0.0001), and EDHB 72h versus BJ (p=0.0002). (F) Production of extracellular lactate in FFs (BJ, SCR-KD, HIF1-KD), FFs transduced with the 4F, hESCs (H1 and H9), and BJ-FFiPSCs (iB4 and iB5). The values are reported to the amount of lactate generated in control wild-type BJ fibroblasts. *p<0.05, two, two-tailed Unpaired Student's t test: 4F 24h versus BJ (p=0.035), 4F 48h versus BJ (p=0.021). **p<0.01, two-tailed Unpaired Student's t test, 4F 72h versus BJ (p=0.008). ***p<0.005, two-tailed Unpaired Student's t test: hESCs versus BJ (p=0.0035), BJ FFiPSCs versus BJ (p=0.0041).

66x74mm (600 x 600 DPI)

Figure 7

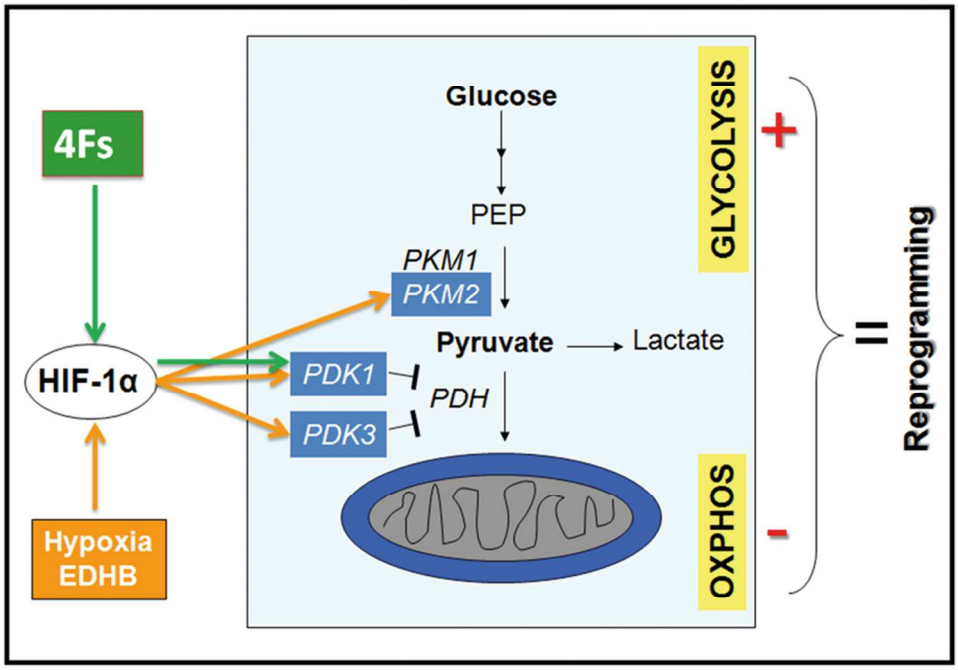

Figure 7. HIF1α-associated metabolic reconfiguration during reprogramming initiation.
Cartoon depicting the potential mechanisms through which the introduction of the 4F or the modulation of HIF1α pathway might regulate glycolytic metabolism during the early stages of somatic cell reprogramming. The introduction of the 4F in somatic fibroblasts up-regulates the HIF1α target PDK1, which re-routes the energy flux outside the mitochondria, thereby enhancing the glycolytic metabolism. HIF1α activation up-regulates additional HIF1α targets PKM2 and PDK3, further increasing the glycolytic shift and eventually resulting in improved conversion to pluripotency.
47x39mm (600 x 600 DPI)

Supp. Fig.1

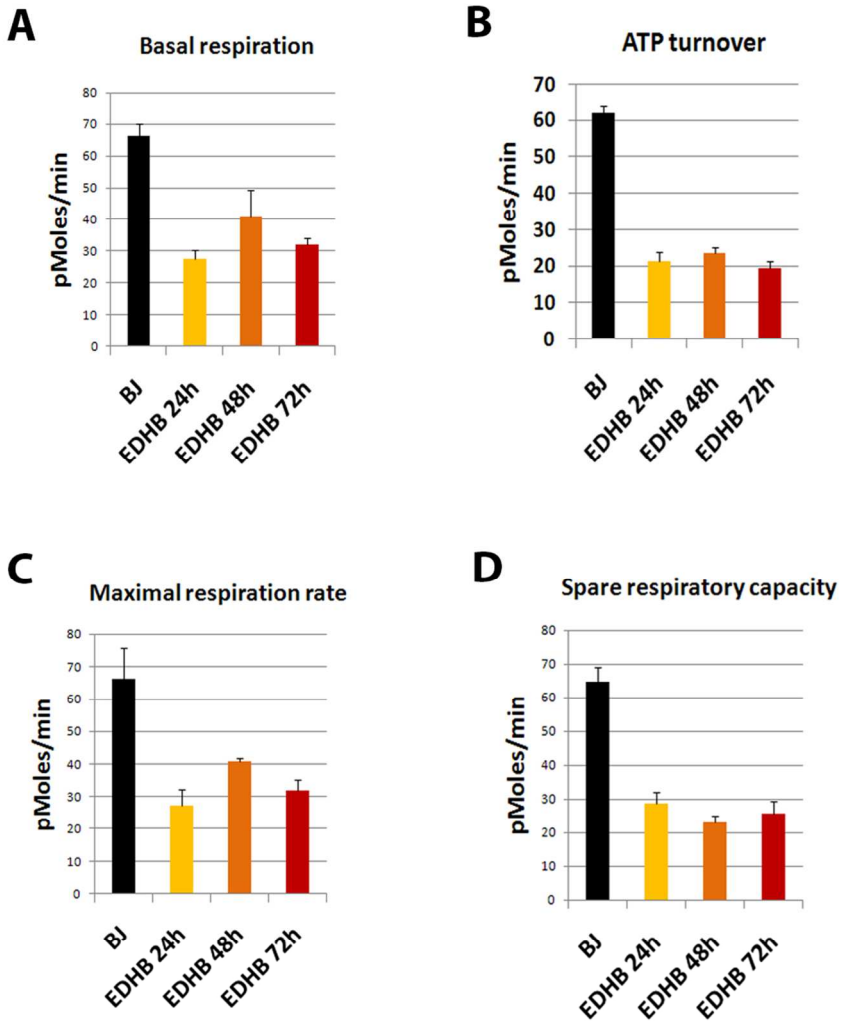

Supp. Figure 1. (A) Basal respiration in BJ fibroblasts and in BJ fibroblasts treated for three days with 500μM EDHB was calculated by subtracting the OCR values following rotenone and antimycin A treatment from the basal OCR values. (B) ATP turnover was estimated by subtracting OCR measurements after oligomycin introduction from the basal OCR measurements. (C) Maximal respiration rate was calculated by subtracting the OCR values after rotenone and antimycin a exposure from the OCR values after FCCP exposure. (D) Spare respiratory capacity was estimated by subtracting the basal OCR measurements from OCR measurements following FCCP injection.
74x102mm (600 x 600 DPI)

Supp. Fig. 2

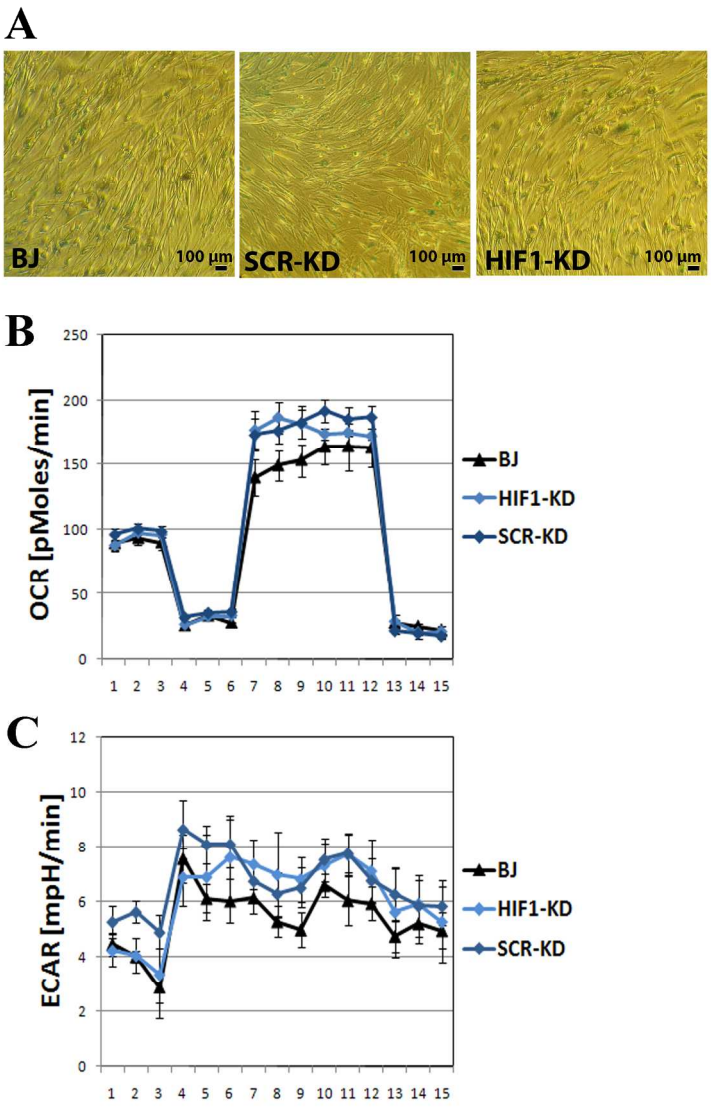

Supp. Figure 2. (A) Neonatal foreskin fibroblasts BJ were transduced with lentiviruses containing shRNA sequences against human HIF1α (BJ-HIF1-KD) and scrambled control oligonucleotides (BJ-SCR-KD). The transduced cells maintained fibroblast-like growth features and did not display signs of senescence, as shown by lack of β-galactosidase staining. (B) OCR profile of BJ, SCR-KD, and HIF1-KD fibroblasts. (C) ECAR profile of BJ, SCR-KD, and HIF1-KD fibroblasts.
145x237mm (600 x 600 DPI)

Supp. Fig. 3

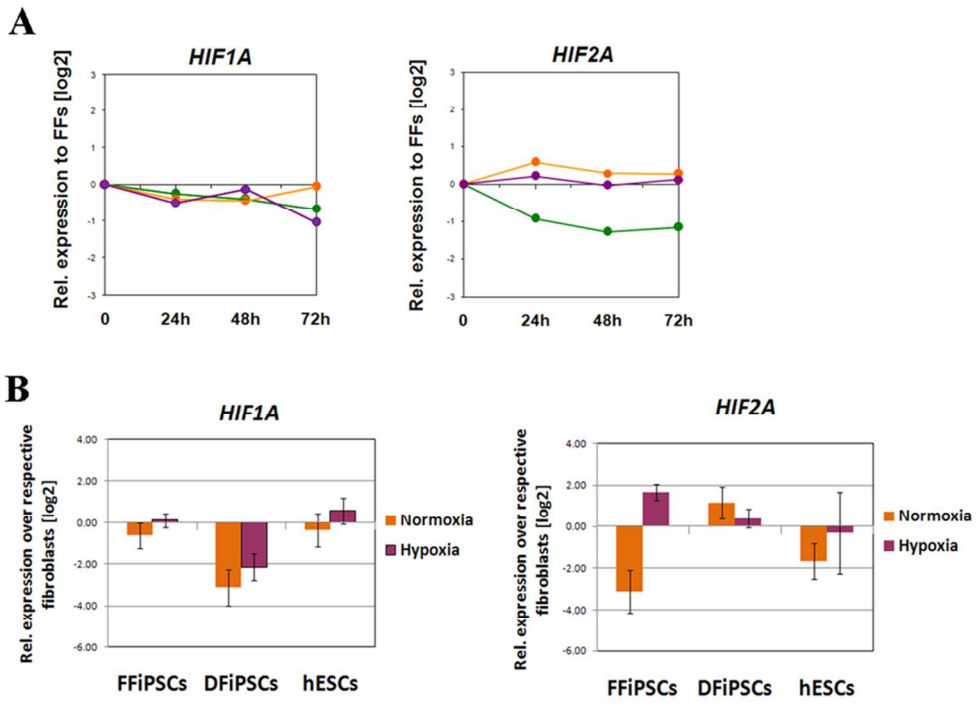

Supp. Figure 3. (A) HIF1A and HIF2A expression level in FFs following 4F transduction and/or EDHB treatment. (B) HIF1A and HIF2A expression level in normoxic and hypoxic FFiPSCs, DFiPSCs, and hESCs in relation to normoxic FFs, DFs, and FFs + DFs, respectively.
45x37mm (600 x 600 DPI)

Supp. Fig. 4

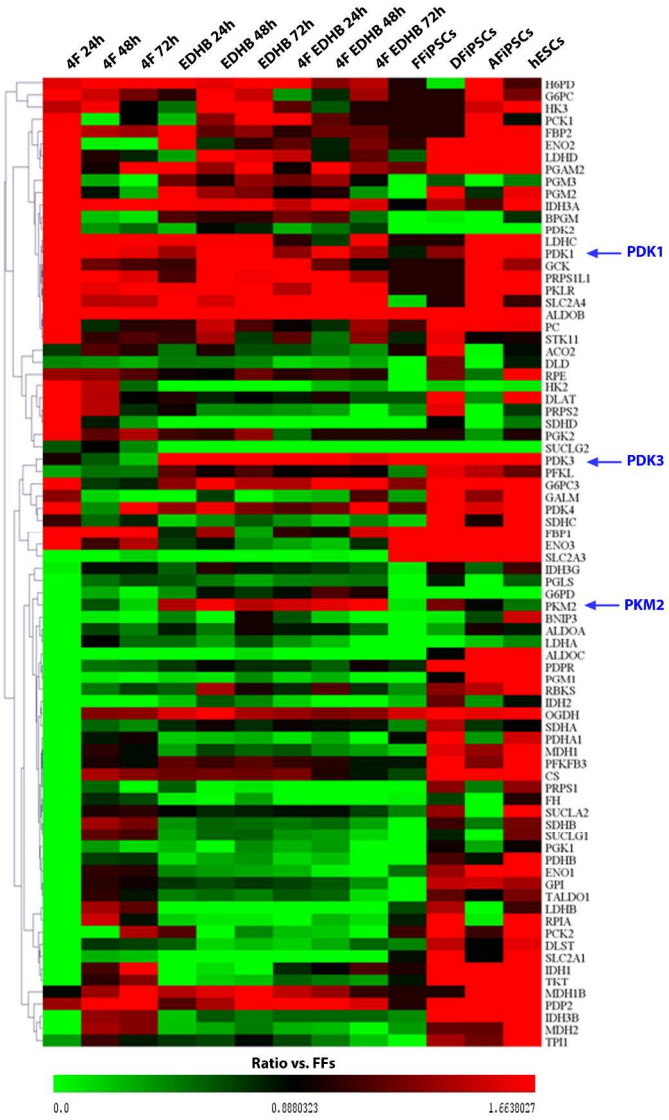

Supp. Figure 4. Heatmap and clustering of genes involved in energy metabolism (list taken from the Human Glucose Metabolism PCR Array). Values represent the ratio over wild-type untreated FFs; down-regulated genes are indicated in green, up-regulated genes in red. PDK1, PDK3, and PKM2 are shown with blue arrows.
383x649mm (300 x 300 DPI)

	TargetID	SCR-KD.AVG_Signal	HIF1-KD.AVG_Signal	HIF-KD.Diff Pval
1	HIF1A	840.37	148.78	7.82E-13
2	PPFIA4	84.86	15.87	1.48E-02
3	CX3CR1	165.06	36.21	8.46E-05
4	ZBTB7A	119.43	28.36	1.04E-02
5	A2M	363.17	88.63	3.16E-08
6	TNFRSF1(	178.66	43.82	1.36E-04
7	PTHR1	216.62	54.33	6.49E-06
8	AMOT	103.90	26.69	1.22E-02
9	HSPB3	1847.28	519.46	8.05E-11
10	CCND2	414.99	117.53	3.03E-08
11	MMP11	2446.98	711.70	8.47E-09
12	TPP2	179.72	55.40	8.52E-03
13	COMP	81.98	25.84	4.69E-02
14	C1ORF19(	85.02	27.07	4.28E-02
15	COL8A2	572.80	182.80	6.20E-07
16	RARB	198.53	63.56	2.41E-03
17	LRRC32	357.85	118.34	8.01E-06
18	SLC24A3	169.56	56.95	2.20E-03
19	SPINT2	684.61	230.24	1.60E-06
20	RNF212	87.82	30.08	4.76E-02
21	MARK1	354.36	124.31	1.47E-06
22	UCN2	90.20	32.54	4.31E-02
23	ERMP1	227.06	86.23	1.75E-03
24	CST6	99.11	37.73	3.67E-02
25	SUSD2	200.96	76.64	9.41E-04
26	CCDC109E	704.32	269.38	3.33E-05
27	EXTL1	165.32	63.56	3.42E-03
28	FAIM3	160.53	62.84	4.42E-03
29	PPP1R14A	710.25	279.08	1.04E-06
30	DRD1IP	141.03	55.42	1.29E-02
1	RSAD2	5.00	728.98	3.68E-38
2	IL8	5.00	277.53	1.03E-11
3	IFI27	211.69	7817.48	3.68E-38
4	CMPK2	5.00	183.86	5.60E-08
5	SST	5.00	174.17	1.52E-06
6	IFI44L	133.28	4235.28	3.68E-38
7	OAS1	28.77	853.60	2.05E-23
8	SLC39A8	5.00	124.54	6.84E-05
9	HERC5	116.68	2846.25	3.68E-38
10	LRRC17	5.00	106.51	1.92E-04
11	CYP1B1	97.30	1777.36	3.68E-38
12	TMEFF2	6.58	119.41	1.17E-04
13	SLC16A6	6.57	106.72	9.43E-04
14	OAS2	217.19	2963.19	3.88E-22
15	LGALS9	5.00	60.47	2.24E-02
16	GNA14	11.17	135.00	3.86E-05
17	BST2	69.97	815.40	4.44E-16
18	MX2	339.01	3924.26	8.88E-16
19	HERC6	464.37	4422.53	3.68E-38
20	ZNF804A	10.26	95.11	2.59E-03
21	DTX3L	23.64	205.78	2.83E-07

22	ESM1	38.48	329.90	6.30E-11
23	EPSTI1	847.96	7178.81	3.68E-38
24	RTP4	32.05	269.82	2.35E-09
25	OASL	29.40	240.89	1.80E-06
26	MX1	4012.46	32269.70	3.68E-38
27	C6ORF192	36.24	273.41	1.66E-09
28	HCP5	109.21	819.36	2.22E-16
29	CLDN1	152.92	1132.21	1.36E-12
30	DDX58	186.47	1368.32	3.68E-38

HIF1-KD/SCR-KD ratio	LOG2 ratio
0.18	-2.50
0.19	-2.42
0.22	-2.19
0.24	-2.07
0.24	-2.03
0.25	-2.03
0.25	-2.00
0.26	-1.96
0.28	-1.83
0.28	-1.82
0.29	-1.78
0.31	-1.70
0.32	-1.67
0.32	-1.65
0.32	-1.65
0.32	-1.64
0.33	-1.60
0.34	-1.57
0.34	-1.57
0.34	-1.55
0.35	-1.51
0.36	-1.47
0.38	-1.40
0.38	-1.39
0.38	-1.39
0.38	-1.39
0.38	-1.38
0.39	-1.35
0.39	-1.35
0.39	-1.35
145.80	7.19
55.51	5.79
36.93	5.21
36.77	5.20
34.83	5.12
31.78	4.99
29.67	4.89
24.91	4.64
24.39	4.61
21.30	4.41
18.27	4.19
18.15	4.18
16.24	4.02
13.64	3.77
12.09	3.60
12.09	3.60
11.65	3.54
11.58	3.53
9.52	3.25
9.27	3.21
8.70	3.12

8.57	3.10
8.47	3.08
8.42	3.07
8.19	3.03
8.04	3.01
7.54	2.92
7.50	2.91
7.40	2.89
7.34	2.88

20fold up	FF	DF	AFCs	FFiPSCs	DFiPSCs	AFiPSCs	hESCs
TUBB2B	339.4	107.8	1127.1	13008.9	25569.1	35359.8	55087.2
CCND2	92.1	17.6	709.2	5116.3	8773.9	6650.5	20533.3
RBPMS2	87.3	134.4	123.0	3309.3	9153.0	5955.2	17482.0
APOE	46.7	21.9	158.7	8362.5	17693.0	18141.2	16683.2
CNTNAP2	5.0	14.1	35.7	2766.6	4057.5	3741.5	12686.7
LIN28	5.0	12.9	35.9	2800.2	11011.3	10065.9	11741.5
DPPA4	5.0	15.7	40.2	2141.7	7855.9	5809.9	11455.7
GAL	198.8	24.5	54.0	4259.8	11770.7	3930.1	10287.3
ZIC2	5.0	13.5	40.8	1573.3	2957.0	6490.3	8292.6
MT1G	75.2	32.9	204.3	473.0	3191.4	6615.1	8089.2
CDH1	5.0	20.7	65.7	2584.3	7252.0	5521.5	7060.2
CRABP1	5.0	16.8	38.7	779.6	2887.1	2152.7	7057.5
SCNN1A	5.0	20.1	67.8	928.6	3713.6	3037.8	6772.2
POU5F1	5.0	14.4	36.1	1038.8	4999.3	5339.9	6760.6
PROM1	5.0	14.1	232.9	2697.6	5117.8	4855.7	6227.9
RCOR2	49.4	49.4	75.9	897.8	1601.0	2504.6	5943.8
RASL11B	10.6	29.8	42.7	836.1	2591.0	4721.2	5925.3
ZSCAN10	5.0	11.5	33.6	1469.9	5193.4	6049.5	5893.4
MT1H	5.0	18.7	38.1	279.0	1580.0	3327.6	5868.1
HAND1	5.0	15.0	30.8	5766.4	11434.9	785.2	5609.5
KIF1A	5.0	15.6	40.5	3436.8	6858.1	3385.5	5607.8
CST1	5.0	15.4	44.2	3948.1	2832.4	4543.2	5546.9
GLDC	5.0	20.3	59.6	1505.0	3850.2	4251.2	5465.6
NEFM	22.6	21.2	41.7	555.9	388.7	1049.8	4823.6
SOX2	5.0	12.7	30.3	914.6	1447.5	1383.0	4306.9
LIN28B	5.0	16.2	32.5	832.1	2711.1	1343.8	4007.5
APOA2	5.0	15.1	61.7	1861.8	2970.4	758.4	3948.7
ACTA1	5.0	16.9	44.9	7236.6	16719.8	219.3	3615.6
PUNC	5.0	12.5	30.1	1255.6	2628.9	1730.2	3549.4
RAB17	5.0	29.4	122.4	1379.8	1776.2	3431.8	3407.8
CXADR	5.0	16.3	122.5	1169.0	3344.1	1799.0	3223.9
EPHA1	5.0	15.2	70.5	841.7	2261.7	2649.5	3084.0
MYCN	5.0	17.0	42.8	673.6	3605.8	1445.3	3027.2
GDF3	5.0	17.5	40.3	285.6	431.5	1377.3	2886.6
H19	33.0	18.1	47.7	6223.7	13665.5	500.1	2799.9
ZIC3	5.0	17.5	36.0	509.1	2091.4	897.3	2687.6
EOMES	5.0	14.5	29.6	400.8	680.7	774.7	2572.6
PRSS8	5.0	15.1	42.8	723.8	1129.0	679.8	2563.1
KIF5C	5.0	17.9	41.9	780.3	1700.0	1153.8	2545.8
CHD7	10.3	22.0	96.5	921.8	1390.5	919.8	2523.5
KCNK12	5.0	18.0	51.3	688.4	1401.5	1395.9	2512.2
LCP1	5.0	18.2	39.8	1253.7	2994.7	289.6	2467.5
CAMKV	5.0	17.7	36.5	430.5	1503.6	2172.9	2466.6
LEFTY1	5.0	13.0	40.6	815.7	3523.3	560.7	2464.9
WDR72	5.0	14.8	43.3	25.8	670.6	475.6	2459.9
TRIML2	5.0	16.9	49.8	1098.2	2321.4	1379.0	2415.1
CDH3	5.0	16.5	46.2	1047.2	2437.5	2127.0	2413.2
FLJ22662	10.4	31.5	42.5	279.0	908.7	709.8	2400.5
CLDN7	20.5	24.4	52.9	791.3	2491.1	1341.7	2393.0

NMU	5.0	14.5	34.6	384.2	1791.1	691.0	2387.8
HERC5	10.5	17.3	56.8	339.8	2161.8	806.3	2380.2
NODAL	5.0	23.1	46.2	396.0	1211.6	459.2	2333.0
RPRM	5.0	14.3	33.4	1036.3	3413.1	736.3	2305.3
SALL4	5.0	14.1	45.0	642.5	2792.9	1356.2	2234.3
SOX21	5.0	17.1	53.4	616.2	216.0	2317.5	2226.3
POU5F1P1	5.0	15.9	57.0	1314.8	5942.9	1678.0	2196.1
SBK1	5.0	16.9	44.3	463.9	1268.7	1291.7	2153.2
CGN	5.0	16.4	69.9	934.7	1946.4	1262.1	2064.7
GPM6B	5.0	14.5	35.8	454.0	1277.5	978.4	2044.8
SLC7A3	5.0	16.0	40.0	536.5	1967.4	1326.9	1930.3
D4S234E	5.0	19.5	59.3	528.4	1913.6	1232.8	1921.4
LEFTY2	5.0	15.4	44.6	1300.3	2067.5	283.6	1801.2
VGF	7.5	21.0	77.6	2228.8	5178.8	551.0	1796.6
DLK1	5.0	16.6	46.0	359.8	1405.8	1286.3	1792.6
CRMP1	5.0	17.0	46.7	550.4	1449.6	891.4	1696.1
RIMS3	7.9	16.7	54.7	327.1	588.8	946.9	1686.3
C9ORF135	5.0	16.2	52.1	305.8	1267.4	1154.6	1568.2
LRRN1	5.0	15.9	42.6	456.2	1548.4	1192.4	1508.0
HEY2	5.0	18.7	39.5	414.1	1315.2	602.7	1459.2
SLC16A9	5.0	18.3	47.9	756.3	1028.4	593.2	1440.5
DNMT3B	5.0	24.7	49.0	491.3	3001.0	723.8	1414.2
SOX8	13.1	18.9	51.6	724.7	760.8	1203.9	1412.5
APOA1	5.0	15.1	39.2	2125.8	2440.7	49.6	1385.1
GLIPR1L1	5.0	20.6	45.2	880.1	2779.3	147.5	1373.4
SYT4	5.0	15.8	34.7	141.2	198.1	202.4	1327.7
CPVL	9.2	21.5	52.7	347.1	1516.0	771.2	1326.6
NELL2	5.0	13.0	41.8	489.6	851.1	914.4	1273.5
L1TD1	5.0	20.9	37.6	860.2	2777.5	509.7	1253.1
SST	5.0	14.3	37.1	73.6	354.1	35.9	1245.3
EDNRB	5.5	23.6	43.7	206.5	620.6	985.3	1241.8
FZD3	5.0	17.2	64.1	283.9	275.2	700.6	1203.3
MIXL1	5.0	15.1	25.5	75.9	201.4	171.7	1161.5
OVOL2	5.0	16.5	41.7	237.0	912.2	885.6	1116.4
SILV	5.0	17.8	57.3	184.0	793.7	1483.8	1106.0
TCEAL2	5.0	17.3	43.8	99.4	883.5	649.1	1081.8
COBL	5.0	16.8	42.4	534.6	1391.9	839.5	1047.1
NKD2	5.0	14.5	28.3	278.2	548.1	992.1	1030.9
C1ORF187	5.0	11.6	46.7	453.8	870.8	463.8	942.9
SLC35F1	5.0	13.4	32.8	299.6	277.8	390.8	913.2
RPRML	5.0	20.1	38.3	196.5	375.3	449.0	906.3
FOXA2	5.0	12.6	34.6	158.5	275.8	461.1	877.7
MMP9	5.0	11.5	26.7	455.6	2178.8	464.9	857.9

4F 24h	4F 48h	4F 72h	EDHB 24h	EDHB 48h	EDHB 72h	4F EDHB 24h	4F EDHB 48h
216.2	718.2	1641.7	161.5	198.7	175.4	202.8	168.7
57.1	83.9	223.4	309.6	203.9	202.8	156.8	172.3
100.9	179.9	170.7	145.8	132.6	114.9	115.4	97.6
109.7	96.0	169.5	110.3	87.3	60.8	65.3	57.6
11.6	5.3	9.1	9.2	12.6	15.1	5.2	6.4
13.2	5.0	5.7	5.0	10.4	11.4	5.0	6.4
21.5	24.2	29.5	11.1	17.3	16.6	7.6	9.3
769.7	1034.0	1468.5	571.3	247.4	215.4	252.5	202.0
21.1	19.9	21.8	14.9	19.0	19.5	14.0	23.6
162.1	167.6	1972.1	264.4	95.8	111.6	168.6	154.2
20.9	22.7	23.2	14.2	17.6	17.9	13.6	14.9
14.6	12.0	11.5	7.7	16.0	13.4	12.2	15.8
18.7	24.9	39.5	13.9	18.1	16.4	11.1	12.6
1306.8	2477.8	2265.9	7.8	12.1	13.4	231.2	446.0
16.4	11.0	20.7	5.0	11.8	10.0	5.3	5.0
73.2	153.0	189.0	25.1	31.8	37.3	28.9	28.5
27.9	29.6	30.3	29.3	37.0	31.9	36.1	20.7
10.1	13.1	11.7	14.2	12.8	11.7	6.2	5.0
23.0	45.2	1233.8	16.9	23.6	22.1	28.6	19.5
120.2	283.7	705.0	6.8	16.1	15.7	15.5	15.2
11.2	5.0	8.0	6.2	12.6	16.7	15.2	7.6
12.0	19.5	28.2	27.6	12.1	16.4	17.2	11.5
21.5	30.5	43.3	19.0	13.2	16.5	14.9	11.5
74.6	83.4	60.9	47.5	31.1	35.6	35.8	58.9
13.1	13.2	10.7	8.1	10.6	7.9	12.1	7.2
10.4	7.9	9.1	21.8	18.9	18.1	37.0	26.7
22.4	18.5	18.3	10.8	21.8	14.5	10.7	14.1
21.3	18.8	22.1	11.1	15.0	16.2	7.4	16.6
15.0	19.0	21.0	6.7	14.9	9.3	12.8	7.4
22.9	21.8	15.4	17.8	20.9	21.2	20.8	16.2
10.1	18.8	69.9	14.4	10.1	14.7	14.0	13.6
20.4	20.8	20.3	17.3	14.9	19.3	13.4	6.3
6.8	5.5	7.8	13.2	22.4	15.0	16.5	11.5
18.2	18.2	36.1	13.2	14.4	13.6	11.3	14.4
1338.0	1263.8	2359.2	39.4	44.3	39.2	476.2	804.3
5.0	10.5	12.2	24.4	13.7	27.1	19.3	13.1
9.1	5.0	5.0	11.8	14.0	22.3	18.8	12.5
9.9	5.0	9.7	16.3	18.6	23.4	11.1	12.1
28.2	16.8	18.4	16.1	22.0	21.0	33.0	38.0
29.7	45.5	58.5	37.9	34.4	34.3	43.0	36.7
23.7	34.2	40.9	18.3	24.7	19.4	13.4	10.8
14.1	13.8	13.8	21.3	19.1	11.2	13.1	8.6
18.1	52.2	46.3	16.8	25.2	24.4	21.4	25.1
7.3	10.8	9.6	10.6	13.3	13.9	10.3	7.7
7.9	13.4	6.6	6.6	8.1	21.8	5.5	5.0
27.5	43.7	121.0	23.1	17.3	19.8	16.0	8.4
18.6	17.3	21.8	17.8	16.1	21.6	15.3	14.4
33.5	39.5	67.2	31.7	28.0	24.2	25.7	27.5
65.1	68.2	112.3	15.5	22.1	18.1	12.8	19.9

10.3	8.3	15.6	11.2	13.9	17.1	7.6	9.5
884.0	548.7	272.7	34.6	45.5	45.7	2108.4	3806.9
22.0	14.3	14.9	21.1	30.2	29.2	15.8	25.7
20.0	19.8	28.1	8.7	16.9	13.2	15.4	6.4
10.7	13.6	29.5	10.9	12.4	17.7	7.1	14.3
22.6	29.6	62.8	11.1	16.8	15.6	5.5	12.3
1712.9	2822.4	2695.6	8.0	14.5	16.4	364.0	589.2
13.2	12.8	17.0	17.6	12.2	16.9	15.4	21.1
9.3	83.6	116.1	17.3	14.1	17.6	19.5	18.7
17.9	23.1	26.1	18.3	15.0	17.9	7.5	14.4
17.3	12.0	16.1	13.2	15.8	15.3	11.2	14.7
76.1	482.6	778.9	27.6	31.4	28.7	34.5	33.1
17.1	17.7	20.1	15.2	20.3	18.3	7.1	13.2
52.8	61.1	66.9	61.4	40.4	34.2	36.3	43.2
25.9	36.1	77.8	11.2	12.4	11.6	9.0	9.1
19.5	22.9	45.0	17.1	18.0	23.9	17.3	16.7
19.2	15.2	18.3	27.9	21.0	25.0	34.6	30.6
17.2	29.9	164.2	9.8	18.9	23.6	6.6	12.3
12.3	14.5	13.4	16.3	17.8	18.4	16.6	13.2
15.6	11.4	13.1	12.6	16.8	13.3	14.0	15.2
18.7	64.8	67.2	13.5	14.6	18.0	6.9	30.3
22.5	23.6	24.1	24.3	20.1	20.2	30.1	24.1
269.7	316.6	214.6	90.3	101.6	99.1	69.7	73.4
9.5	5.2	6.6	8.5	15.6	19.7	11.6	9.5
21.5	29.8	25.0	18.8	18.3	22.5	17.2	27.2
6.8	5.0	5.2	10.9	17.7	14.2	16.7	13.2
27.0	28.6	25.9	24.8	24.7	25.4	18.1	17.4
12.2	11.6	20.0	8.6	13.8	15.7	10.6	12.3
58.5	191.2	169.3	18.8	22.4	27.7	35.6	33.9
18.8	23.2	45.2	31.7	20.4	19.8	13.0	12.9
18.2	22.0	24.6	23.2	21.4	21.4	20.6	20.5
15.9	8.1	12.2	11.4	17.5	22.3	18.7	10.2
5.0	9.7	12.3	6.1	7.8	11.8	9.7	5.1
14.3	14.6	15.6	10.7	16.9	18.5	14.5	16.9
11.9	9.3	9.3	21.4	26.1	22.6	18.6	23.8
13.4	13.3	17.0	23.7	14.7	21.7	17.5	15.6
14.9	19.2	26.2	17.5	15.2	14.1	20.0	12.9
13.9	15.0	19.1	7.2	14.2	13.6	5.0	5.0
22.9	28.9	16.2	9.6	17.1	15.9	9.1	11.5
18.3	12.1	14.0	11.4	15.7	29.6	15.4	11.1
16.0	60.0	290.8	19.8	21.4	18.1	16.5	17.0
5.0	8.1	10.6	10.9	14.0	12.7	9.8	8.0
7.0	5.0	14.6	12.5	14.0	19.6	5.2	6.5

4F EDHB 72h	HIF KD	SCR KD
219.0	343.6	460.6
297.1	71.1	231.0
100.3	162.0	110.3
27.6	43.2	59.6
10.9	5.0	10.3
5.3	6.4	10.8
5.1	9.5	9.1
119.4	31.3	15.9
16.8	10.2	10.8
141.5	42.5	54.0
5.0	29.7	23.2
5.0	6.1	13.3
11.9	12.1	16.7
635.7	7.1	9.9
7.9	5.0	5.4
32.5	22.6	36.8
13.5	21.0	34.6
5.0	6.3	8.4
20.9	16.0	22.1
11.2	5.0	7.5
5.0	15.6	10.0
15.0	9.6	5.0
27.4	10.6	14.3
28.4	35.2	23.3
5.8	5.5	5.0
21.0	9.0	26.0
15.3	11.0	15.9
12.7	10.5	10.1
5.0	10.3	12.9
19.6	10.3	23.2
13.8	7.1	6.9
7.9	13.0	10.9
15.0	19.8	13.2
16.7	8.9	7.2
552.1	25.2	44.6
9.3	22.7	22.9
18.9	17.8	25.7
6.2	10.1	11.3
24.3	30.8	18.9
33.2	28.0	23.4
20.7	6.4	13.2
13.3	6.0	11.4
16.0	18.0	11.2
9.0	5.0	5.0
5.0	9.5	5.2
13.8	19.6	12.2
8.4	5.7	10.2
23.3	53.6	28.1
27.3	25.6	15.6

5.1	10.0	5.5
4005.4	1606.9	73.2
29.8	17.7	14.7
21.3	6.5	10.9
5.7	6.9	19.3
14.9	11.9	14.0
794.5	5.0	9.1
14.1	23.8	22.3
7.4	12.4	14.6
10.1	6.7	10.7
7.9	12.3	7.6
41.6	22.5	15.3
19.4	14.2	13.4
49.2	37.4	29.1
8.5	8.3	9.4
10.3	15.4	15.8
22.5	24.9	30.2
8.2	9.5	13.0
12.8	11.4	9.7
14.1	24.7	19.4
12.1	13.6	7.7
23.7	18.0	16.2
46.1	65.4	61.3
24.3	9.1	5.0
13.4	22.0	7.7
15.9	6.3	7.5
15.3	13.7	22.4
5.0	5.5	7.2
11.9	15.7	16.9
12.6	102.9	7.5
29.0	24.7	23.0
16.3	11.6	8.0
6.9	5.0	5.0
9.7	10.5	11.5
14.4	18.5	15.1
11.2	10.6	10.0
9.2	10.0	14.0
14.7	9.7	5.0
8.5	6.3	9.1
11.1	8.7	15.1
14.8	13.2	7.1
6.2	6.7	9.9
5.0	5.8	9.8

20fold down	FF	DF	AFCs	FFiPSCs	DFiPSCs	AFiPSCs	hESCs	4F 24h
S100A4	13232.4	10700.6	1570.3	272.9	116.4	599.6	755.9	31915.7
GAS6	3257.3	5060.1	10132.6	755.2	784.2	395.9	668.5	2155.7
THBS1	10621.6	11184.0	24606.4	360.2	1153.6	213.2	659.2	7614.5
CSRP1	2569.5	1766.9	10485.4	1657.9	2792.9	332.7	611.8	2833.8
S100A6	5227.8	3670.5	3668.2	1383.4	1979.2	212.2	588.5	7096.0
CD248	7733.8	5426.3	79.1	314.5	458.0	106.0	574.5	16411.3
ARID5B	2697.2	1775.7	2751.3	271.7	420.5	87.8	519.6	2192.3
IGFBP3	4565.3	6262.1	3919.3	1226.9	2316.5	95.9	477.0	4744.4
WNT5A	2731.9	622.6	162.1	187.0	336.8	46.2	365.3	952.4
RGS4	421.0	1189.6	11568.9	259.6	648.6	43.0	352.9	1357.2
LOX	3986.9	3456.7	6793.6	328.8	365.9	115.4	341.4	9462.5
LMCD1	1699.8	1109.1	340.1	391.1	601.2	127.1	283.3	440.9
SULF1	5348.4	1000.3	2034.6	233.5	281.9	93.7	266.4	6054.0
SELM	1112.4	1130.0	2151.7	147.1	369.2	253.2	244.0	1463.8
LOXL4	2259.0	3321.4	2887.3	329.9	165.7	71.8	235.5	1580.8
CTSK	2363.4	2575.5	82.7	70.5	125.6	123.3	226.4	3420.3
COL8A1	561.5	2139.0	6143.9	212.7	85.9	56.6	203.9	500.9
CYBRD1	3283.3	2920.1	1274.3	63.4	135.8	101.7	200.5	2607.3
DCN	6763.8	3410.5	1069.9	56.4	494.2	21.6	175.3	5640.2
TIMP3	2265.2	718.0	51.8	283.4	395.0	38.9	170.8	3099.3
LAYN	1212.2	1085.2	889.8	97.8	208.2	72.4	168.0	1072.2
FBLN5	1882.6	1367.9	98.8	123.9	236.7	38.3	162.1	1480.3
PPP1R3C	1503.5	959.3	1295.9	50.8	190.0	115.1	160.7	3236.0
MVP	884.6	1037.3	1561.6	123.8	194.7	88.4	159.6	1182.7
VEGFC	888.6	806.7	2155.3	104.9	169.7	42.6	157.5	1666.6
ADAMTS1	1032.1	197.6	610.7	207.3	321.0	51.2	137.1	703.5
GLIPR1	645.3	1216.6	3680.8	194.4	141.3	17.2	135.4	1667.0
NFIX	1640.8	4939.3	2000.1	497.8	284.6	209.5	133.8	1757.2
OXTR	3322.0	2615.2	3039.4	128.4	196.9	40.6	122.8	2058.0
ITGA11	202.2	1110.1	3293.8	33.5	35.5	25.8	121.1	61.7
NNMT	1124.3	692.4	905.0	130.9	177.6	58.9	118.5	556.9
CPA4	668.6	323.6	17227.5	86.0	40.5	15.3	116.6	205.0
COL16A1	1330.1	537.6	374.7	184.4	149.1	58.1	115.0	1205.6
CRYAB	778.6	1988.8	1956.9	89.3	2382.0	44.9	113.9	1240.4
TNFRSF14	704.5	574.6	90.9	110.0	136.1	70.2	105.2	857.0
TMEM119	2630.9	5938.3	32.0	96.6	119.6	33.4	101.6	1331.3
HOXA5	126.5	192.4	4540.1	139.3	331.8	52.5	99.9	182.1
COL12A1	1052.9	1099.0	312.3	79.9	115.0	32.9	93.5	396.3
NTN4	888.5	112.5	911.6	86.7	88.4	48.2	91.1	286.3
LRP10	627.6	748.2	697.6	131.9	289.3	74.1	89.2	640.7
FAP	1556.7	1103.9	1897.9	17.1	15.3	16.0	86.7	1333.5
CERCAM	521.0	776.3	1038.6	100.6	196.7	63.5	84.4	377.6
TMEM173	878.5	1300.9	2365.8	43.3	244.3	18.7	81.6	1424.4
MFAP5	1339.5	1635.4	964.9	383.6	302.6	31.7	79.7	581.9
RCN3	1274.3	650.2	313.0	42.3	61.0	72.5	74.5	2102.8
ANPEP	1809.1	2382.6	951.1	134.2	428.9	26.2	74.0	2569.7

LY96	877.3	477.8	138.1	50.9	32.2	48.2	71.5	1613.1
FSTL3	298.9	172.1	1767.4	136.6	313.0	59.4	70.6	304.4
ENG	593.6	954.6	741.4	58.4	94.8	59.0	69.9	1070.1
TNFRSF11B	2533.7	785.7	921.8	48.6	28.3	21.9	67.2	1970.6
MEG3	1467.2	1121.8	3933.1	378.3	4668.7	272.5	67.0	2262.5
C1R	1381.3	570.4	56.9	10.5	29.8	78.8	61.2	910.1
CD97	522.6	608.4	786.1	184.0	211.8	195.9	60.4	775.2
ABCC3	594.4	351.8	269.4	100.1	134.3	36.8	58.1	374.7
IFIT2	428.6	112.9	82.2	46.7	160.6	36.3	57.8	3046.5
KIAA1199	6731.8	2543.6	131.5	28.6	151.6	22.2	57.6	2919.8
RECK	1050.0	409.6	174.7	47.1	31.8	13.1	57.1	887.2
NUPR1	775.1	730.0	39.4	63.2	167.6	33.4	56.8	697.8
C1S	895.9	426.0	42.1	21.7	65.2	59.5	56.4	664.4
MYLK	719.8	448.7	319.7	29.3	53.7	35.8	55.5	485.7
MGLL	377.5	301.5	528.9	24.9	39.4	40.5	54.7	622.7
C1QTNF5	395.0	744.5	63.9	42.8	79.8	62.2	50.3	334.8
C10ORF116	825.2	1163.2	109.8	17.3	532.7	39.1	48.3	2660.1
GREM1	638.5	352.6	246.0	54.0	7.6	27.9	46.7	477.9
COX7A1	858.2	1122.1	54.7	32.8	676.2	41.2	44.5	685.9
C15ORF52	955.9	848.5	2540.0	79.8	59.2	37.1	43.0	1576.4
FOXF2	397.0	88.3	52.8	36.9	41.0	33.9	42.6	355.2
TRIM4	494.1	318.8	392.8	137.8	168.2	217.7	38.4	655.5
GPNMB	1137.0	1241.4	50.5	5.0	511.7	37.6	37.1	1252.3
NOV	457.6	163.2	75.7	15.7	26.8	25.4	37.1	619.1
HSPB6	337.8	1148.4	1050.7	17.4	156.2	43.5	36.9	483.8
COPZ2	376.2	252.1	301.0	12.7	21.6	27.8	36.1	711.4
LUM	499.6	85.0	63.5	46.9	39.7	18.6	36.0	202.9
P8	612.3	514.8	48.6	50.2	120.7	19.7	35.5	680.7
UBA7	302.1	243.9	41.6	18.4	52.5	32.4	34.7	603.1
VGLL3	414.3	482.6	218.4	18.2	46.3	21.9	32.6	158.1
PODN	1567.0	940.3	52.8	16.3	16.6	56.4	31.1	1406.1
HSPB3	569.3	1137.3	219.5	7.9	275.1	32.5	30.0	846.6
MXRA8	286.6	819.7	982.2	18.2	90.7	54.3	29.7	467.2
SRGN	357.6	328.5	5394.7	14.7	19.1	27.7	28.4	260.7
WNT2	235.7	26.4	38.7	10.5	28.5	20.6	28.3	127.7
MMP3	1928.0	751.7	45.7	16.8	22.3	31.1	26.6	2747.4
HSPB7	155.1	888.0	34.5	10.0	58.5	27.8	26.2	442.4
GBP1	267.1	128.0	166.6	12.0	11.3	18.1	19.6	323.4
APOD	478.9	237.6	44.7	6.8	6.2	38.1	17.2	33.6
SERPINB7	524.2	173.5	844.6	6.5	10.2	18.9	17.2	764.6
KRT34	1360.7	68.1	1547.9	5.0	5.0	16.5	17.1	1072.5
CLIC3	114.9	141.9	1304.0	9.6	109.7	18.5	15.5	821.8
SAMD9	341.7	181.8	124.5	22.7	6.2	25.7	15.0	2285.3
PSG6	464.3	63.0	43.4	5.0	33.8	16.4	13.9	437.3
PSG4	570.8	219.9	45.0	13.3	84.8	19.4	12.9	502.3
SYNC1	408.9	411.1	337.8	9.9	10.6	15.0	12.7	411.5
CLEC3B	193.5	364.7	48.0	5.0	5.0	15.7	12.1	87.6

OSR2	297.6	198.8	46.2	5.0	5.0	15.8	10.5	157.6
PSG9	1015.8	353.7	64.5	5.0	29.6	11.9	7.2	990.1
C10ORF54	534.0	98.2	40.9	5.0	25.7	12.7	5.0	271.7

4F 48h	4F 72h	EDHB 24h	EDHB 48h	EDHB 72h	4F EDHB 2⁴	4F EDHB 4⁸	4F EDHB 72	HIF KD
34552.3	30845.8	10239.0	8618.1	9170.1	11680.4	11927.1	8835.0	13935.0
1993.8	1498.0	4723.8	4822.2	5372.9	3597.7	4247.3	3760.0	3980.5
5347.0	4543.8	12956.2	12934.5	16977.9	12391.3	12054.2	5189.0	15306.4
1842.6	1376.7	5633.6	5493.8	7764.8	5079.8	3685.0	2224.8	5308.1
7874.2	6038.2	4847.2	4753.1	5021.0	4851.4	5407.1	5930.5	4446.5
15354.8	9176.0	4089.2	8877.2	9705.7	6929.0	9463.7	9802.8	8869.4
1709.9	1672.6	2072.6	4029.1	3241.1	3132.4	2878.9	2968.0	4020.9
3000.2	1720.8	5444.0	3281.4	4480.9	2618.7	3569.9	1611.4	9084.8
962.4	905.0	1186.6	1605.0	1909.9	1025.4	1081.7	803.2	3499.9
1540.6	716.2	1183.0	740.7	1057.4	1182.6	1631.6	912.9	499.8
7554.0	4519.9	4526.8	3847.7	4958.6	4288.2	4522.3	3532.8	6439.3
922.4	906.9	241.9	614.2	538.4	468.3	576.8	361.1	1800.7
6772.5	5725.6	3515.1	2335.3	2605.5	3006.1	5919.8	3802.4	5485.3
1246.2	1303.5	1214.3	1287.2	1623.2	1186.5	1284.2	1140.2	1653.0
3142.1	2231.7	1165.8	1192.2	1814.6	757.7	981.5	889.6	2260.5
3707.3	3704.5	2787.4	1979.3	1500.7	1344.8	1930.2	2689.6	3675.2
615.4	499.3	444.3	454.5	763.9	295.9	365.2	290.3	1473.8
2605.5	2065.4	3786.5	2743.9	3156.6	3078.0	3055.6	2523.4	4981.5
5687.1	4874.7	4621.7	4754.6	4371.4	3887.8	4777.4	4170.1	4187.8
2312.8	1554.3	4425.5	2844.7	2441.7	2322.1	2252.2	2221.2	2361.5
593.1	506.3	960.8	1547.6	1200.5	1353.8	1230.0	1074.6	2607.8
1259.0	972.1	2209.6	1929.2	2029.8	1691.9	1994.6	1747.6	3858.0
2207.5	2170.8	725.6	828.1	748.3	921.5	1169.2	1720.3	760.7
1125.4	948.1	1070.4	1187.9	1144.6	1257.9	1496.9	1326.7	1149.8
836.1	481.3	3515.6	2898.2	3326.4	3651.1	3686.0	2306.3	1847.9
406.4	234.3	1139.3	1613.9	1595.2	1617.5	1854.4	1032.9	2013.6
913.1	353.0	537.5	687.5	1222.7	913.9	871.5	530.7	643.2
1785.1	1701.0	3617.7	5182.9	4547.1	4027.4	4726.7	4874.9	3946.0
1079.5	468.8	3886.8	4006.2	5131.7	3117.6	2240.6	554.7	4864.9
38.6	49.9	325.4	351.4	331.5	200.6	188.3	136.2	501.6
664.3	820.0	509.6	352.6	559.1	556.3	530.7	513.0	721.7
1057.0	1308.6	238.4	975.0	650.7	610.9	1371.5	1520.8	720.5
1047.7	766.3	517.0	579.3	538.7	479.0	456.0	321.0	965.1
803.7	730.2	1021.2	845.3	554.3	914.7	769.0	345.3	2096.8
1147.3	1185.2	218.0	430.9	313.2	572.3	858.1	923.7	775.3
2710.4	2315.4	858.7	2498.4	1164.3	1323.1	1111.2	1628.1	1308.3
248.2	283.7	178.2	173.1	159.7	161.2	208.9	293.2	115.9
282.2	203.8	1138.0	1366.5	1307.9	975.2	898.1	719.3	1271.8
293.5	332.9	683.9	670.4	701.7	685.0	1054.1	1107.5	3011.6
507.6	351.9	725.7	824.6	889.3	778.2	961.4	907.6	1273.0
1303.6	1266.8	1893.6	1283.2	1264.5	1415.1	1333.1	1059.3	1559.1
397.6	358.6	1254.5	1411.3	1094.4	883.7	1171.9	1242.8	1123.7
965.1	773.5	1581.3	1638.2	1074.5	2362.1	2767.0	2044.9	2625.0
500.7	463.5	1457.6	1263.9	1209.9	1035.6	857.0	330.8	1034.6
1847.9	1036.1	789.9	728.7	872.9	842.8	830.7	806.0	676.7
1842.7	1096.9	6225.7	4570.9	3733.6	3220.1	4313.3	5640.8	1527.1

1980.1	2123.0	1270.1	824.1	863.5	1134.7	1769.3	2452.9	1512.7
200.3	181.5	815.0	535.7	623.0	595.4	436.6	191.0	850.2
948.4	568.6	1098.2	908.1	830.1	728.1	1081.2	977.0	847.4
1401.4	868.8	2753.3	2367.7	3283.8	2320.0	2648.4	1197.5	4721.1
2127.7	2390.1	1464.4	1647.1	2235.9	1701.6	2306.1	3507.8	1410.6
1369.1	1666.0	822.6	598.8	515.4	947.7	1584.5	2136.3	1351.4
859.0	662.1	810.5	1019.3	836.6	1039.4	999.8	838.2	649.6
266.8	182.0	534.7	627.2	770.9	729.5	884.4	569.7	506.0
1895.7	936.2	195.4	315.9	287.8	11365.8	15835.1	13331.8	4781.6
2974.8	2832.4	2483.9	4204.3	3042.4	3222.5	2157.5	1033.6	7861.0
713.9	523.0	445.0	468.3	501.5	300.5	395.5	264.9	630.2
567.9	1359.3	401.4	191.7	220.9	446.8	448.5	635.2	1029.2
936.7	1117.7	794.6	577.7	445.9	826.6	1371.0	1621.5	1458.8
324.8	212.9	833.8	956.3	890.7	776.8	900.6	806.8	1117.9
436.1	299.6	753.2	398.4	468.5	453.5	440.9	260.6	503.7
306.5	412.1	303.2	276.1	180.0	358.4	226.8	240.4	633.1
3804.1	3972.9	1213.3	1643.7	1158.1	1536.5	2078.5	2161.9	833.8
298.2	170.2	339.9	224.8	357.6	466.8	469.8	167.3	605.3
536.5	468.8	1220.3	1120.6	1207.2	1021.4	1073.1	961.0	1648.8
1317.8	1023.2	961.0	1235.2	1000.4	1048.3	1192.8	848.1	1400.4
389.0	332.9	371.9	462.4	332.7	395.7	399.5	403.8	459.9
713.0	627.9	566.0	598.4	564.0	578.6	678.9	734.4	705.8
1405.1	1560.2	1751.2	1009.9	732.3	1151.4	1873.6	2600.8	2088.0
654.3	402.4	340.5	347.8	247.0	539.9	883.4	627.0	1380.7
413.1	285.8	965.7	855.3	914.1	1025.3	1120.3	920.3	1011.0
583.3	444.4	324.2	399.7	432.7	326.3	390.3	383.1	431.8
200.0	174.3	164.1	161.6	195.9	159.2	230.8	119.0	325.5
454.4	1074.0	367.8	171.8	162.0	373.9	356.3	475.9	721.8
846.0	448.4	75.5	187.2	101.8	474.1	1031.4	912.4	457.2
143.3	135.7	167.2	256.7	387.3	138.9	103.2	52.1	368.1
1209.4	1144.4	1335.6	938.3	837.2	670.2	658.3	581.2	2453.2
994.9	792.8	41.4	161.7	132.5	207.2	202.0	60.3	297.3
310.0	247.8	576.9	237.6	870.5	921.9	923.8	954.0	714.3
176.0	73.4	698.7	638.8	758.2	648.2	635.6	448.3	658.3
157.3	154.4	28.9	43.4	45.1	34.3	40.4	29.1	125.5
1497.6	419.4	2032.8	1622.2	1693.0	2350.8	2639.9	2357.0	2522.1
136.8	62.4	466.0	322.9	384.6	417.2	245.4	62.4	542.2
328.5	207.0	78.6	153.9	206.0	858.6	1005.9	640.9	1032.1
78.4	158.2	1680.1	1242.1	849.4	558.3	772.4	1143.1	720.5
408.7	189.7	741.6	849.8	1044.7	928.4	716.3	362.9	570.6
444.3	167.8	5326.0	1788.6	5096.9	3200.5	2824.6	639.4	3219.3
428.3	665.2	68.0	175.3	147.9	225.7	316.3	86.7	210.7
2598.3	1610.9	311.2	396.4	357.7	2241.6	3487.8	3279.9	1119.0
290.4	146.0	203.5	161.4	185.9	163.3	222.4	170.9	266.1
331.4	175.7	539.7	438.0	536.8	424.8	518.7	467.0	632.7
288.8	275.8	152.2	225.9	287.4	267.3	220.8	137.6	659.6
131.5	293.8	51.9	74.5	75.5	57.7	59.2	77.8	115.3

135.3	138.8	224.2	374.0	287.0	329.3	393.5	264.6	622.4
509.5	249.7	786.9	677.4	847.5	754.9	922.8	672.4	1043.4
639.6	793.7	37.4	83.5	55.3	53.9	81.6	84.8	340.3

SCR KD
13290.7
4898.7
18392.0
6086.7
4531.3
7051.6
4359.1
6436.2
3411.9
382.5
5403.1
2069.9
8296.7
1995.8
1480.8
4712.5
813.7
6212.9
5112.2
1782.6
1882.5
3064.8
1428.7
1227.0
1824.4
1822.0
514.4
5590.3
5317.8
994.0
1082.4
563.4
1172.9
2552.6
652.6
2877.7
153.2
1768.7
2210.6
1226.9
2636.6
1401.9
2120.4
1956.2
711.9
1712.1

1194.5
952.5
827.9
3610.9
1567.7
1105.0
632.0
617.9
729.9
7799.9
755.0
915.6
1067.8
1216.6
408.3
1258.9
839.5
553.0
1989.7
1594.6
495.4
643.3
2880.8
791.7
1261.1
420.1
239.4
693.8
204.1
459.4
3063.2
989.1
915.9
518.5
66.7
1153.6
889.2
292.7
663.3
513.0
4036.5
192.1
409.7
353.0
827.5
461.7
106.9

792.2
1366.6
264.8

		LOG2 ratio PSCs over respective somatic cells				LOG2 ratio
Pathway	**Gene**	**FFiPSCs**	**DFiPSCs**	**AFiPSCs**	**hESCs**	**4F 24h**
HIF pathway	*HIF1A*	-1.32472	-0.14476	-2.12118	-0.33018	-0.24648
	HIF2A	-1.277	0.254546	-1.86007	-1.828	-0.92826
	HIF3A	0	-1.13546	-1.0079	1.314304	1.163173
	EGLN1	-0.26675	0.478343	-1.22186	0.86345	0.167642
	EGLN2	0.022896	1.667587	-0.05731	1.715912	1.114057
	EGLN3	1.906598	1.243785	-0.36449	3.20434	1.727792
Glucose metabolism	*SLC2A1*	0.838216	3.37233	-0.63902	1.871524	-0.38918
	SLC2A3	3.161092	3.626333	2.593632	4.471338	-0.43842
	SLC2A4	0.134897	-1.75626	-0.68636	1.073538	1.337318
	LDHA	-1.24821	-0.02246	-1.02373	0.413997	0.956869
	LDHB	0.628746	2.743092	0.090048	1.080396	0.501023
	LDHC	0	-1.63573	-0.82699	3.544952	2.456882
	LDHD	0.552873	1.392309	1.449535	2.97693	0.871806
	PFKL	0.425188	1.103037	-0.43161	1.211234	0.339445
	PFKFB3	0.814285	1.978096	-0.94773	1.675069	0.532532
	PKM2	0.085242	0.751188	-1.08879	0.475667	0.590584
	PKLR	0	-1.70998	-0.69799	1.914589	1.808865
	PDK1	0.784813	-0.05158	-0.82282	2.652892	1.738163
	PDK3	2.023877	3.236353	0.831652	4.456384	0.434946
	ENO2	1.037563	2.01967	0.312073	3.221445	-0.08439
	ALDH9A1	-0.52749	0.810336	-0.35254	1.29554	0.075207
mTOR/Autophagy	*BNIP3*	-1.23455	0.632964	-0.98902	1.523424	-0.06827
	IDH1	0.993386	2.532364	2.035234	3.016112	0.42
	REDD1	1.514988	3.078718	2.104921	2.840165	0.19
	FRAP1	1.095095	2.114259	0.840836	2.367248	0.64
	RICTOR	0.731814	-0.14735	-0.91735	1.556596	1.06
	TSC1	-0.29518	1.328942	-0.46117	-0.08845	-0.07
	TSC2	1.188298	1.42713	-0.30013	0.937955	-0.05
	EIF4B	0.342956	1.912345	1.411853	2.134099	-0.09
	LKB1	0.759724	0.849671	-0.56368	0.964241	0.60
	ATG5	-0.55435	1.08134	0.224307	1.397168	0.25
	ATG7	-0.69998	0.666393	-0.76789	0.784888	1.08
	ATG10	0.870945	1.724113	1.012972	3.084164	0.79
	ATG12	-0.2937	1.31414	-0.25749	1.569154	0.71

over FFs

4F 48h	4F 72h	EDHB 24h	EDHB 48h	EDHB 72h	4F EDHB 24h	4F EDHB 48h	4F EDHB 72h
-0.38949	-0.67326	-0.39634	-0.43809	-0.04532	-0.50406773	-0.12097651	-1.03524687
-1.2843	-1.16017	0.59213	0.294654	0.279806	0.216882601	-0.02755145	0.128134197
1.283967	1.227399	1.340147	1.668346	2.044068	1.357834604	1.41566349	1.366241071
0.688618	0.395339	0.689773	0.817407	1.337671	0.853578267	1.16068642	0.513313759
1.590191	1.407596	-0.14252	-0.52898	-0.45133	-0.13779387	-0.20269747	-0.18205001
2.178325	2.205649	0.875938	1.640353	1.692109	1.278640207	1.18186458	1.53463737
0.271099	0.214724	-0.3357	-0.50101	-0.04558	-0.29474642	-0.55226665	-0.76993463
-0.14209	0.160589	-0.59201	-0.59818	-0.00459	-0.23783633	0.05951629	-0.20992319
1.470044	1.482445	1.850267	1.563047	2.14463	1.730640825	2.15870283	1.707071503
0.87278	0.521507	0.515879	0.319926	0.61524	0.380431993	0.2305529	0.002761306
1.387434	1.176448	-0.69524	-0.66801	-0.66674	-0.45201987	-0.60491799	-0.61229165
2.208933	2.471894	1.633983	2.231059	2.106531	1.026447397	0.67308817	2.383168443
0	0.766061	0.32238	1.707187	1.600474	1.4896611	0.78809214	1.188007121
0.492777	0.474184	1.188152	0.946982	1.131325	0.911373767	0.96938046	0.91618633
0.978268	0.861875	1.193726	1.070762	1.171731	1.063587487	1.01879591	0.813540497
0.599438	0.163701	1.42983	1.658813	1.462483	1.535814579	1.60359922	1.790236794
1.612614	1.688279	1.659283	1.847028	1.920683	1.451551383	1.8176871	1.765805438
1.721297	1.619517	1.381037	1.78312	1.951815	1.323538461	1.71571916	1.393300736
0.584895	0.215747	1.794389	1.868575	1.962995	1.993684507	1.92576498	1.592561741
0.044764	-0.02124	1.880062	0.696102	1.049519	1.182336225	0.77853425	1.272774798
0.221064	0.136057	0.119773	0.022001	0.341679	0.054686503	0.13760004	0.13757899
0.06712	-0.15464	0.426042	-0.06127	0.954506	0.589615216	0.17958938	-0.11082864
1.115855	1.767397	-0.02526	0.110223	-0.05926	0.742687069	0.88580219	1.131558358
0.753582	2.14973	-0.68675	-0.91987	-1.30265	-0.75639503	-0.63174354	1.042291129
0.57796	0.766775	1.112215	1.111626	1.009241	0.813621373	0.95210913	0.79393086
1.342604	1.03313	1.827893	2.02331	2.126559	2.233730879	2.08670539	1.674324834
0.033172	0.068781	-0.66091	-0.2974	-0.4351	-0.57644638	-0.48441901	-0.2228336
-0.021	-0.12102	1.113446	1.695776	0.999762	0.977921037	0.79208675	1.220387482
0.443335	0.658392	-0.03136	0.073874	0.040324	-0.05730454	-0.14019292	0.098470173
1.052762	1.14325	1.067682	1.423491	0.694329	1.170153203	0.48430684	1.330947419
0.513042	0.658055	-0.38546	-0.55282	-0.19185	-0.32225646	-0.61126102	-0.3129495
1.096352	0.981186	-0.30869	-0.17181	-0.21949	-0.26713564	-0.00075836	0.010926037
0.452965	0.876907	1.079918	0.760891	0.89901	0.973226302	0.57335314	0.82930881
0.848512	0.445102	0.135664	-0.36603	0.208828	0.428855037	0.52201342	0.474980525

	LOG2 ratio over SCR-KD fibroblasts
	HIF1-KD
	-2.36353
	-0.47953
	-0.46067
	-0.81644
	0.323768
	-0.59355
	-0.43584
	-0.87866
	0.501852
	-0.29101
	0.039252
	-0.47357
	0.017723
	-0.31976
	0.083061
	-0.34047
	1.047267
	0.045597
	-1.048
	-1.09335
	-0.53001
	-0.65086
	0.014818
	-0.58453
	0.133109
	-0.83028
	0.565405
	-0.10668
	-0.55512
	-0.8339
	0.20546
	0.1318
	-0.03871
	0.329465

Supp. Table 4. List of primers used for real-time QPCR analysis

Gene	Forward sequence (5'-3')	Reverse sequence (5'-3')
ACTB	TCAAGATCATTGCTCCTCCTGAG	ACATCTGCTGGAAGGTGGACA
PDK1	ACTTCGGATCAGTGAATGCTTG	ACTCTTGCCGCAGAAACATAAA
PDK3	CGCTCTCCATCAAACAATTCCT	CCACTGAAGGGCGGTTAAGTA
PKM2	AAGGACCTGAGATCCGAACTG	GCGTTATCCAGCGTGATTTTGA
HIF1A	GGCGCGAACGACAAGAAAAAG	CCTTATCAAGATGCGAACTCACA
HIF2A	CTCTCCTCAGTTTGCTCTGAAAA	GACAGAAAGATCATGTCGCCA